

**FEDERAL UNIVERSITY OF ITAJUBÁ**  
**MECHANICAL ENGINEERING INSTITUTE**

**WAVELET TRANSFORM-BASED DAMAGE IDENTIFICATION IN  
LAMINATED COMPOSITE BEAMS**

**GUILHERME ANTONIO OLIVER**

**ITAJUBÁ - MG**

**2021**

**FEDERAL UNIVERSITY OF ITAJUBÁ**  
**MECHANICAL ENGINEERING INSTITUTE**

**WAVELET TRANSFORM-BASED DAMAGE IDENTIFICATION IN  
LAMINATED COMPOSITE BEAMS**

**Guilherme Antonio Oliver**

**A dissertation presented to the Post-graduate Program of Mechanical Engineering, from Mechanical Engineering Institute of the Federal University of Itajubá, as a requirement to obtain the title of Master in Mechanical Engineering**

**Advisor: Guilherme Ferreira Gomes**

**Co-advisor: Antonio Carlos Ancelotti Junior**

**ITAJUBÁ - MG**

**2021**

*This work is dedicated to my parents,  
for all the support given during these years.*

# Acknowledgements

I thank my parents for all the support, affection, encouragement and teachings during my life. Nothing would be possible without you.

To my girlfriend, thank you for the companionship, love and patience during this journey.

My dissertation advisor, Guilherme Gomes, accompanied this work with willingness and enthusiasm and was always available to share his scientific knowledge, to make suggestions, to encourage and inspire not only me, but all of his students. I thank you for this.

I would like to thank Antonio Ancelotti, my dissertation co-advisor and all professors and staff from UNIFEI for contributing to my academic education and making this work possible. I also thank all colleagues from GEMEC for the shared knowledge and for the great moments I've had while working with you.

Finally, to my brothers from Francisco Maselli 779, it was a pleasure to live with you.

*“If you want to find the secrets of the universe,  
think in terms of energy, frequency and vibration.”*

*— Nikola Tesla*

# Abstract

Laminated composite structures suffers from delamination, the detachment of the layers due to the rupture of the fiber-matrix interface, as their principal mode of failure. Differently from other damages, such as cracks, delaminations are often not visible on the surface causing a late detection and leading to sudden failures. To ensure that laminated composite structures operate flawlessly, precise monitoring methods are required. The present study proposes a damage index to identify delaminations in a laminated composite beam, yet, the development is based on a well-defined methodology. The proposed damage index is composed of a weighted sum of Discrete Wavelet Transform detail coefficients, obtained by applying the transform to the mode shapes of the structure. Numerical models of the beams with a stiffness reduction in limited areas to simulate damage, provided data for tuning the coefficients of the damage index by performing a mixture design analysis and a multiobjective optimization. After substantial results for identifying damage in numerical cases, the damage index efficiency was tested with real carbon fiber-reinforced polymer beams. The experimental specimens were manufactured with delaminations induced by embedding non-sticking films between the layers. Again, substantial results in identifying damaged were achieved. The damage index proved to be efficient to locate damage in almost all positions along the beam. It is important to emphasize that the proposed damage index is a no-baseline method, a method that does not require information of the pristine structure. Finally, this study performs a deep statistical analysis on the effects of damage characteristics, such as position and severity, in a damage identifying technique. The results of the analysis serves as basis for developing more sophisticated and optimized damage identifying methods.

**Keywords:** Damage Identification. Wavelet Transform. Structural Health Monitoring. Delamination. Composites.

# Resumo

Estruturas de material compósito tem as delaminações, o descolamento das camadas do laminado devido ao rompimento da interface fibra-matriz, como seu principal modo de falha. Diferentemente de outros danos, como trincas, muitas vezes as delaminações não são visíveis na superfície, o que causa uma detecção tardia e pode levar a falhas repentinas e catastróficas. Para garantir que essas estruturas funcionem perfeitamente, são necessários métodos precisos de monitoramento da integridade estrutural. O presente estudo propõe um índice de dano para identificar delaminações em uma viga fabricada em material compósito, porém, com desenvolvimento baseado em uma metodologia bem definida. O índice de dano proposto é composto por soma ponderada dos coeficientes de detalhe da Transformada Wavelet Discreta, obtidos pela aplicação da transformada aos modos de vibração da estrutura. Modelos numéricos das vigas foram criados usando a redução da rigidez em áreas limitadas para simular danos, estes modelos forneceram dados para ajuste dos coeficientes do índice de dano feito por meio de um arranjo de misturas e de uma otimização multiobjetivo. Após resultados substanciais para identificação de danos em casos numéricos, a eficiência do índice de dano foi testada com vigas reais em fibra de carbono. Os corpos de prova foram fabricados com delaminações induzidas pela incorporação de filmes antiaderentes entre as camadas. Mais uma vez, o índice de dano se mostrou eficiente para localizar danos em quase todas as posições ao longo da viga. É importante enfatizar que o índice de dano proposto é um método que não requer informações da estrutura original sem danos. Este estudo também realiza uma análise estatística dos efeitos das características do dano, como posição e severidade, na identificação do dano. Os resultados da análise servem de base para o desenvolvimento de métodos de identificação de danos mais sofisticados e otimizados.

**Palavras-chave:** Identificação de Danos. Transformada Wavelet. Monitoramento da Integridade Estrutural. Delaminação. Compósitos.

# List of Figures

Figure 1 – Numerical models of a composite beam with nine different damage locations. The damage was modelled as a local stiffness reduction in a group of finite elements. . . . .	23
Figure 2 – Representation of the Simplex-Lattice Design used in the present study, for two combinations of the six components, with seven degrees. . . . .	24
Figure 3 – Flowchart for the tuning process of the damage index components. . . . .	25
Figure 4 – Bi-orthogonal 3.1 wavelet, the mother wavelet chosen for obtaining detail coefficients of mode shapes. . . . .	26
Figure 5 – Damage index without tuned parameters for a damage level of $\alpha = 0.1$ . . . . .	27
Figure 6 – Results of the simplex-lattice design for damage index parameter tuning. Plotted for the components $D_{1,1} - D_{1,2} - D_{1,3}$ . . . . .	30
Figure 7 – Results of the simplex-lattice design for damage index parameter tuning. Plotted for the components $D_{2,1} - D_{2,2} - D_{2,3}$ . . . . .	31
Figure 8 – Performance plots for the optimization performed with NSGA-II. . . . .	33
Figure 9 – Pareto Front represented for three responses at a time. . . . .	34
Figure 10 – Damage index with tuned parameters for a damage level of $\alpha = 0.1$ . . . . .	35
Figure 11 – Damage index with tuned parameters for a damage level of $\alpha = 0.3$ . . . . .	36
Figure 12 – Damage index with tuned parameters for a damage level of $\alpha = 0.5$ . . . . .	37
Figure 13 – CFRP laminated beam specimens, one intact and eight with induced delaminations in different longitudinal positions. . . . .	41
Figure 14 – Teflon film used to induce delamination being removed after the laminate manufacturing. . . . .	42
Figure 15 – Experimental setup for the modal testing. . . . .	43
Figure 16 – Comparison between the experimental mode shapes and their respective cubic spline approximation. . . . .	44
Figure 17 – Damage index of the eight beams considering induced delamination in different positions. . . . .	46
Figure 18 – Strain fields obtained by Digital Image Correlation. . . . .	47
Figure 19 – Coefficients of the Wavelet Transform applied to strain fields obtained by Digital Image Correlation. . . . .	48
Figure 20 – Illustration of the damage index behavior. The blue area encompasses the area where damage is present, the red area indicates false-positives and the green dot is the peak value of the DI. . . . .	51
Figure 21 – Experimental specimen of the CFRP beam with the delamination highlighted. . . . .	52



Figure 22 – Comparison between the mode shapes of the numerical models and the CFRP specimens. . . . .	54
Figure 23 – Modal Assurance Criterion for comparing numerical and experimental mode shapes. Values close to one indicate high correlation. . . . .	55
Figure 24 – Damage indexes for the components of the CCD design. . . . .	56
Figure 25 – Main effects plot for (a) Area with damage, (b) Area without damage and (c) damage index peak. . . . .	57
Figure 26 – Pareto’s analysis for (a) Area with damage, (b) Area without damage and (c) damage index peak. Parameter A represents damage position and B represents damage severity. . . . .	58
Figure 27 – Response surface plots for (a) Area with damage, (b) Area without damage and (c) damage index peak. . . . .	60
Figure 28 – Dendrogram showing the degree of similarity of the variables and responses. . . . .	61

# List of Tables

Table 1 – Material properties of the composite material, used as inputs in the finite elements software for the laminated beam model. . . . .	23
Table 2 – Mode shapes and natural frequencies of a pristine and a damaged beam model with damage placed in the central position. . . . .	26
Table 3 – Regression coefficients for the fitted regression model of the nine regions, with the presence of damage . . . . .	28
Table 4 – Regression coefficients for the fitted regression model of the nine regions, without the presence of damage . . . . .	28
Table 5 – Model summary table for the fitted regression model. . . . .	29
Table 6 – Natural frequencies of the beam specimens, in Hertz. . . . .	44
Table 7 – CCD design with the input parameters and respective levels. . . . .	51
Table 8 – Natural frequencies (in Hz) of numerical models and experimental specimens. . . . .	53
Table 9 – Response surface model considering two factors and three responses. . .	56
Table 10 – Main results for the analysis of variance. . . . .	57
Table 11 – Model summary table for the response surface models. . . . .	59

# List of abbreviations and acronyms

<i>ANOVA</i>	Analysis of Variance
<i>CCD</i>	Central Composite Design
<i>CFRP</i>	Carbon Fiber Reinforced Polymer
<i>CWT</i>	Continuous Wavelet Transform
<i>DI</i>	Damage Index
<i>DIC</i>	Digital Image Correlation
<i>DWT</i>	Discrete Wavelet Transform
<i>MAC</i>	Modal Assurance Criterion
<i>MD</i>	Mixture Design
<i>MOOP</i>	Multiobjective Optimization Problems
<i>RSM</i>	Response Surface Method
<i>SHM</i>	Structural Health Monitoring
<i>WT</i>	Wavelet Transform

# List of symbols

$\alpha$	Damage severity factor
$\beta$	Coefficients of the response surface
$\lambda$	Eigenvalues
$\nu_{12}$	Poisson's ratio
$\omega$	Natural frequencies
$\Phi$	Eigenvectors
$\psi(t)$	Wavelet function
$\rho$	Density
$\varphi$	Mode Shapes
$a$	Scaling factor for CWT
$b$	Shifting factor for CWT
$E_1$	Young's modulus in longitudinal direction
$E_2$	Young's modulus in lateral direction
$G_{12}$	In-plane shear modulus
$G_{13}$	Transverse shear modulus for shear in 1-3 plane
$G_{23}$	Transverse shear modulus for shear in 2-3 plane
$j$	Scaling factor for DWT
$k$	Scaling factor for DWT
$K$	Stiffness matrix
$m$	Mixture design polynomial degree
$M$	Mass matrix
$N$	Total of points generated in Mixture Design
$p$	Total Mixture Design components
$R^2$	Indicator of model fitness

$S$	Standard Deviation
$s(t)$	Generic signal
$x_i$	Mixture Design components

# Contents

1	INTRODUCTION . . . . .	15
1.1	Research objective . . . . .	17
1.2	Dissertation Outline . . . . .	17
2	PARAMETER TUNING FOR WAVELET TRANSFORM- BASED DAMAGE INDEX . . . . .	19
2.1	Theoretical Background . . . . .	19
2.1.1	Wavelet Transform . . . . .	19
2.1.2	Mixture Design . . . . .	21
2.1.3	Multiobjective Optimization . . . . .	21
2.2	Numerical Methodology . . . . .	22
2.2.1	Numerical Composite Beam Modelling . . . . .	22
2.2.2	Mixture Design Setup . . . . .	22
2.3	Results and Discussion . . . . .	24
2.3.1	Numerical Modal Analysis . . . . .	24
2.3.2	Damage Index . . . . .	24
2.3.3	Mixture Design for Damage Index Tuning . . . . .	26
2.3.4	Optimization Results . . . . .	29
2.4	Conclusion . . . . .	38
3	EXPERIMENTAL DAMAGE IDENTIFICATION IN LAMI- NATED COMPOSITE BEAMS . . . . .	39
3.1	Theoretical Background . . . . .	39
3.1.1	Mode Shape-based Damage Identification . . . . .	39
3.1.2	Digital Image Correlation . . . . .	40
3.2	Experimental Methodology . . . . .	40
3.3	Results and Discussion . . . . .	42
3.3.1	Experimental Results . . . . .	42
3.3.2	Damage Identification for Mode Shapes . . . . .	42
3.3.3	Damage Identification for Strain Fields . . . . .	45
3.4	Conclusion . . . . .	49
4	STATISTICAL ANALYSIS IN DAMAGE IDENTIFICATION USING WAVELET TRANSFORM . . . . .	50
4.1	Introduction . . . . .	50
4.2	Theoretical Background . . . . .	50

4.2.1	Response Surface Method . . . . .	50
4.3	Results and Discussion . . . . .	52
4.3.1	Numerical-Experimental Validation . . . . .	52
4.3.2	Analysis of Variance . . . . .	53
4.3.3	Response Surface Analysis . . . . .	58
4.4	Conclusion . . . . .	61
5	GENERAL CONCLUSION . . . . .	62
6	PUBLICATIONS . . . . .	64
	Bibliography . . . . .	65
	APPENDIX	70
	APPENDIX A – OBJETIVE FUNCTIONS . . . . .	71

# 1 Introduction

Composite materials are known for their excellent mechanical properties, low weight and their workability in the manufacturing process. Other features of composite materials are corrosion resistance, excellent surface finish and good fatigue strength, which makes it an outstanding choice for applications that need high performance. Since composite materials are a combination of material components, they maintain the advantages of each component and may also overcome weaknesses of its single components [1]. In contrast, it has a complex mechanism of failure which is affected by several effects [2]. Some damage mechanisms are cracking, delamination, fiber breakage etc. [3].

Such damages are not easily detected during visual inspections due to being invisible on the surface, to avoid sudden failures they need to be monitored constantly. This is achieved through Structural Health Monitoring (SHM) techniques [4], that combine sensing technology to intelligent algorithms in order to diagnose the structural condition [5].

Damage identification has been a widely explored topic in structural health monitoring. The identification can be segmented in four levels: judgement, localization, severity and residual lifetime estimation [6]. The problem can be analysed via dynamic responses of the structure usually obtained with vibration analysis, however, other approaches have been studied [7].

Vibration-based methods are extensively used for providing inputs in SHM techniques due being a non-destructive testing and being relatively easy to perform. Through vibration analysis, dynamic characteristics as natural frequencies and mode shapes are obtained and used as inputs on inverse methods for damage identification that can be improved when working together with optimization algorithms, artificial neural networks or wavelet transform. [8].

A common way to identify damage is to develop an damage index where high values indicate its presence. This approach has been applied to several areas: Kim *et al.* [9] used a damage index based on dissipated energy in moment-deformation to quantify the failure criteria for a carbon steel pipe elbow, the most vulnerable part of piping systems. Boursier *et al.* [10] used a damage index technique in combination with finite element method: experimental results were used to set up a finite element model of a composite plate subjected to bending test and the index was used to map the residual elastic properties of the damaged plate. Zhang *et al.* [11] developed a damage index to classify the damage of a long-span prestressed double-layer composite torsional reticulated shell structure in four levels: intact, slight damaged, medium damaged, seriously damaged and collapsed.

Some tools are necessary to develop damage indexes and the Wavelet Transform



(WT) has been widely used in SHM applications, especially no-baseline methods. Ashory *et al.* [12] proposed quantitative methods for selecting suitable wavelets based on the characteristics of the analysed signal, replacing the trial and error approach for choosing the wavelet function. Yang *et al.* [13] applied a 2D Continuous Wavelet Transform (CWT) to the modal frequency surface of a composite laminate plate, obtained by using Finite Element Analysis on a numerical model and successfully identified damage even when noise was added to the data, proving the robustness of wavelet transform. Zhou *et al.* [14] applied 2D CWT to the operating deflection shape of composite laminates with cutouts and verified great results regarding using this more easily obtainable input. Katunin *et al.* [15] used WT to enhance the sensitivity of shearography, a non-destructive testing method, overcoming the problem of small damage detectability. Zhu *et al.* [16] proposed a continuous wavelet transform-based damage index to locate cracks in beams made of functionally graded materials, and an intensity factor to estimate damage extent. Araujo dos Santos *et al.* [17] used a discrete wavelet transform to post-process modal rotation fields in a damage identification method, the discrete wavelet transform provides higher sensibility and has better computational efficiency than other wavelet transform variations. Xu *et al.* [18] made a contribution by evaluating the capacity of 2D Wavelet Transform to characterize non-uniform cracks. Real and complex wavelets were applied to modal curvatures under noisy conditions. Only the complex wavelet was completely capable of eliminating noise interference and clearly locate the damage. Several other papers were published using wavelet-based methods. Abdulkareem *et al.* [19] used WT decomposition in mode shape difference between damaged and undamaged plates to locate damage, then, combined artificial neural networks and WT in a technique to quantify damage severity. Sha *et al.* [20] proposed a method based on teager energy operator together with WT that is able to pinpoint the locations of multiple damages even in noisy environments, this was achieved even without a reference of the pristine structure. The efficiency of WT in no-baseline methods was the reason why it was chosen as the main tool in this study. Some other studies were performed with wavelet-based methods [21, 22], proving its versatility.

A noteworthy thing for structural damage detection problems based on wavelet transform is that the multi-level decomposition performed by the transform generates several coefficients with different levels of importance. Knowing how to rank these coefficients is of extremely importance in the damage identification process, avoiding the detection of false positives or negatives. For this reason, this study introduces a new approach to weight optimization through design of experiments using mixtures design. The result of the methodology employed significantly improved the defined damage index.

In the same way, optimization techniques are another widely used tool in damage identification problems. It can be used in different stages of damage identification methods [23, 24, 25, 26]. In the present study, a multiobjective optimization is used for tuning the weights of the coefficients in the proposed damage index. Generally, multiobjective

optimization problems (MOOP) can be solved using classic techniques, as Weighted Objectives Method [27], which converts a MOOP into a single objective optimization problem or through multiobjective evolutionary algorithm techniques, which find multiple solutions simultaneously [28].

Another method that is currently being used in damage identification studies is the Digital Image Correlation (DIC). Gomes *et al.* [29] developed an inverse algorithm based on strain fields for damage identification in composite plate structures. Wavelet Transform has been associated with DIC technique [30, 31] but the studies approached damage identification in concrete, which has completely different mechanisms of failure from composite materials. The absence of studies involving DIC and WT applied to composite structures motivated the attempt to identify damage using these techniques in the present study.

## 1.1 Research objective

As presented in the Introduction (Chapter 1), composite structures require structural health monitoring techniques to ensure that sudden failures do not occur. The primary objective of this research is to develop a damage identification technique for laminated composite beams using Wavelet Transform as main tool. The mode-shapes of the beam are used as source of data for the proposed method.

Because this objective is broad, it allows other studies and analysis to be carried out during the research. Therefore, some secondary objectives were set to guide the research and are listed below:

- Develop the damage identification technique so that it is a no-baseline method.
- Define the methodology used to create and optimize the damage index, specifying all steps of the process.
- Assess the possibility of using strain fields obtained through Digital Image Correlation as source of data for damage identification.
- Provide a deep statistical analysis on the efficiency and behavior of the proposed damage index.

## 1.2 Dissertation Outline

This dissertation is organized as follows:

- 
- Chapter 2 presents the whole process of developing the damage index with the Wavelet Transform, including the methodology for tuning the parameters.
  - Chapter 3 presents the application of the optimized damage index to experimental specimens in order to evaluate its efficiency. It is also presented an attempt to identify damage through strain fields of the same specimens.
  - Chapter 4 presents a deep statistical analysis in damage identification problems. It also presents the validation for the numerical-experimental methodologies used in the present study.
  - Chapter 5 concludes the dissertation with an overview of the main conclusions and suggestions for future works.

# 2 Parameter Tuning For Wavelet Transform-Based Damage Index

In this chapter, the process of development for the damage index used in this study is presented. The procedure requires a model of the laminated composite beam under analysis, that was modelled using a finite element analysis software. Using a numeric model allows the position and severity of the damage to be changed easily, generating a large set of data for the optimization of the index.

The mode shapes obtained numerically are decomposed by the wavelet transform into levels and each level of each mode shape contributes differently to the damage index. For the index to achieve good efficiency, it is necessary to determine the appropriate weighting of each factor. To do so, a mixture design analysis evaluates the weight distribution and generates regressions which are used as objective functions. Through an optimization, the best combination of weights is found, maximizing the efficiency of the damage index.

The chapter is organized as follows: Section 2.1 provides the theoretical background on the topics of Wavelet Transform, Mixture Design and Multiobjective Optimization. Section 2.2 presents the numerical methodology used for modelling the laminate composite beam and the mixture design. Section 2.3 presents the results of the numerical modal analysis followed by the formulation of the damage index, it is discussed how the mixture design analysis and the multiobjective optimization were conducted and finally the results of the damage identification in the numerical models is presented and discussed. Finally, in Section 2.4 the conclusions are drawn.

## 2.1 Theoretical Background

### 2.1.1 Wavelet Transform

The wavelet transform (WT) is a mathematical tool for signal processing, it highlights features of a signal, enabling details to be seen. As the Fourier transform, WT decomposes signals into combinations of basis functions. The difference is that WT can use various basis functions and Fourier transform uses only sine and cosine functions [32].

According to [33], a wavelet function (denoted as  $\psi(t)$ ) must meet three criteria:

- It must have a zero mean.
- It must have finite energy.

- The Fourier Transform of complex wavelets must be real and vanish for negative frequencies.

There is a wide variety of wavelet functions that can be used in research applications. For example: The Daubechies functions, the Haar functions, the Hat functions, the Hermit cubic functions [34]. Each wavelet function has its own advantageous features and the researcher must test which one works better for the determined research.

There are two manipulations applied to wavelet functions: Shifting, which is moving the wavelet along the  $x$ -axis (represented by the factor  $b$ ) and scaling, which is stretching and compressing the wavelet ( represented by the factor  $a$ ). A wavelet function modified by these two factors has the form  $\psi\left(\frac{t-b}{a}\right)$ .

More specifically, WT can be divided into Continuous Wavelet Transform (CWT) and Discrete Wavelet Transform (DWT). The CWT procedure is exhibited in Eq. 2.1, where  $s(t)$  is the analyzed signal and  $\frac{1}{\sqrt{a}}$  is a energy normalisation factor.

$$CWT(a, b) = \frac{1}{\sqrt{a}} \int_{-\infty}^{\infty} s(t) \cdot \psi\left(\frac{t-b}{a}\right) dt \quad (2.1)$$

In a CWT there is a infinite number of possibilities for scaling and shifting factors. In a DWT, the  $a$  and  $b$  factors are limited to a set of possibilities, shown in Eq. 2.2, where  $j$  is the wavelet scaling factor and  $k$  the wavelet shifting factor.

$$\begin{aligned} a &= 2^{-j} \\ b &= 2^{-j}k \\ j, k &= 0, 1, 2, \dots \end{aligned} \quad (2.2)$$

The procedure of a DWT, is shown in Eq. 2.3.

$$DWT(j, k) = 2^{-\frac{j}{2}} \sum_{-\infty}^{\infty} s(t) \cdot \psi\left(2^{-j}t - k\right) \quad (2.3)$$

Although the name *discrete*, DWT is also used to analyze continuous signals [35], it just does the analysis at specific scales and positions. Another important point is that even though the signal is usually presented as a function of time, the WT can be applied to signals that vary through any quantity. In the present study, the signal is the mode shape, which varies through the length of the structure.

Discrete wavelet transform will decompose the signal into detail and approximation coefficients. The approximation coefficients contain information of the low-frequency components while the detail coefficients contain the high-frequency components. For damage identification applications, the detail coefficients contain the desired information [36].

As DWT uses only a limited scaling and shifting factors, it is computed faster than the CWT. Thus, it will be used for obtaining the detail coefficients for the proposed damage index.

### 2.1.2 Mixture Design

In statistics, the Response Surface Methodology (RSM) is a technique for modelling and analyzing problems that involves expressing a response variable as an empirical function of one or more quantitative factors [37]. In a Mixture Design (MD), a class of RSM, the components  $x_i$  are proportions and obey the constraint  $\sum x_i = 1$ . The form of a quadratic mixture model is exhibited in Eq. 2.4

$$E(y) = \sum_{i=1}^p \beta_i x_i + \sum_{i < j} \sum_{i < j}^p \beta_{ij} x_i x_j \quad (2.4)$$

There are different possible designs in this method, for example: Simplex-Centroid, Simplex-Lattice and Extreme Vertices. In the Simplex-Lattice design, used in the present study, the  $x_i$  components are proportions equally spaced from 0 to 1. This design is defined by  $p$ , which is the total of the components and  $m$ , the degree of the polynomial. Equations 2.5 and 2.6 present the components proportions and the total of points generated in a simplex lattice design [38].

$$x_i = 0, \frac{1}{m}, \frac{2}{m}, \dots, 1 \quad i = 1, 2, \dots, p \quad (2.5)$$

$$N = \frac{(p + m - 1)!}{m!(p - 1)!} \quad (2.6)$$

### 2.1.3 Multiobjective Optimization

According to Rao [39], a multiobjective optimization problem consists in the procedure exhibited in Eq. 2.7.

$$Find \mathbf{X} = \begin{Bmatrix} x_1 \\ x_2 \\ \dots \\ x_n \end{Bmatrix} \quad (2.7)$$

Which minimizes :  $f_1(\mathbf{X}), f_2(\mathbf{X}), \dots, f_k(\mathbf{X})$

Subject to :  $g_j(\mathbf{X}) \leq 0, j = 1, 2, \dots$

where the vector  $\mathbf{X}$  contains  $n$  variables to be optimized,  $f_k(\mathbf{X})$  are the  $k$  objective functions to be minimized and  $g_j(\mathbf{X})$  are the  $j$  inequality constraints. Both the objective functions and the inequality constraints may be nonlinear functions.

Usually, there is not a vector  $\mathbf{X}$  capable of minimizing all  $k$  objective functions simultaneously. In a multiobjective optimization, several feasible solution vectors known as Pareto optimum solutions are obtained. A vector  $\mathbf{X}$  is considered a Pareto optimum solution if there is no other vector that would reduce an objective function without causing a simultaneous increase in at least one other objective function.

## 2.2 Numerical Methodology

### 2.2.1 Numerical Composite Beam Modelling

The numerical model of a composite laminated beam with 27 centimetres of length and 3 centimetres of width was modelled in a Finite Element Analysis software. The composite material is a Carbon Fiber-Reinforced Polymer whose mechanical properties are presented in Table 1. The laminated beam has four layers oriented at  $0^\circ$  and each layer has a thickness of 0.3 mm.

The beam is divided into  $6 \times 54$  finite elements. Each element has eight nodes with six degrees of freedom, three of translation and three of rotation. On one end of the beam all nodes are supported and movement is fully restricted in all six degrees of freedom, which gives the beam a cantilever configuration.

There are some possibilities for modelling damage in a composite structure. Yang *et al.* [13] specified the delamination in a numerical model as two planes (the composite laminated layers) with the same coordinates but that are not tied together. Gomes *et al.* [40] simulated damage in a element by a reduction in its stiffness matrix. The element stiffness matrix  $K_i$ , is multiplied by a constant  $\alpha$  resulting in a new stiffness matrix  $K_{damaged} = \alpha K_i$ . This approach was chosen for the present study due its capacity to vary damage intensity.

Groups of  $6 \times 6$  elements received a reduction in stiffness since reducing in a single element causes changes in the mode shapes too small to be relevant. Altogether, nine possible damage locations were formed, as shown in Figure 1. For each possible damage location, three models were created, with stiffness reductions  $\alpha$  of 0.1, 0.3 and 0.5.

### 2.2.2 Mixture Design Setup

The present study used a six-component Simplex-Lattice Design with a degree of seven. This design was chosen due being adequate to model the weights applied to the coefficients of the damage index. The six components are the wavelet coefficients generated by a two-level decomposition of the first three numerical mode shapes, as explained in Section 2.2.1. This design resulted in a total of 799 combinations considering the augmentation with axial and central points, such high quantity of combinations is not

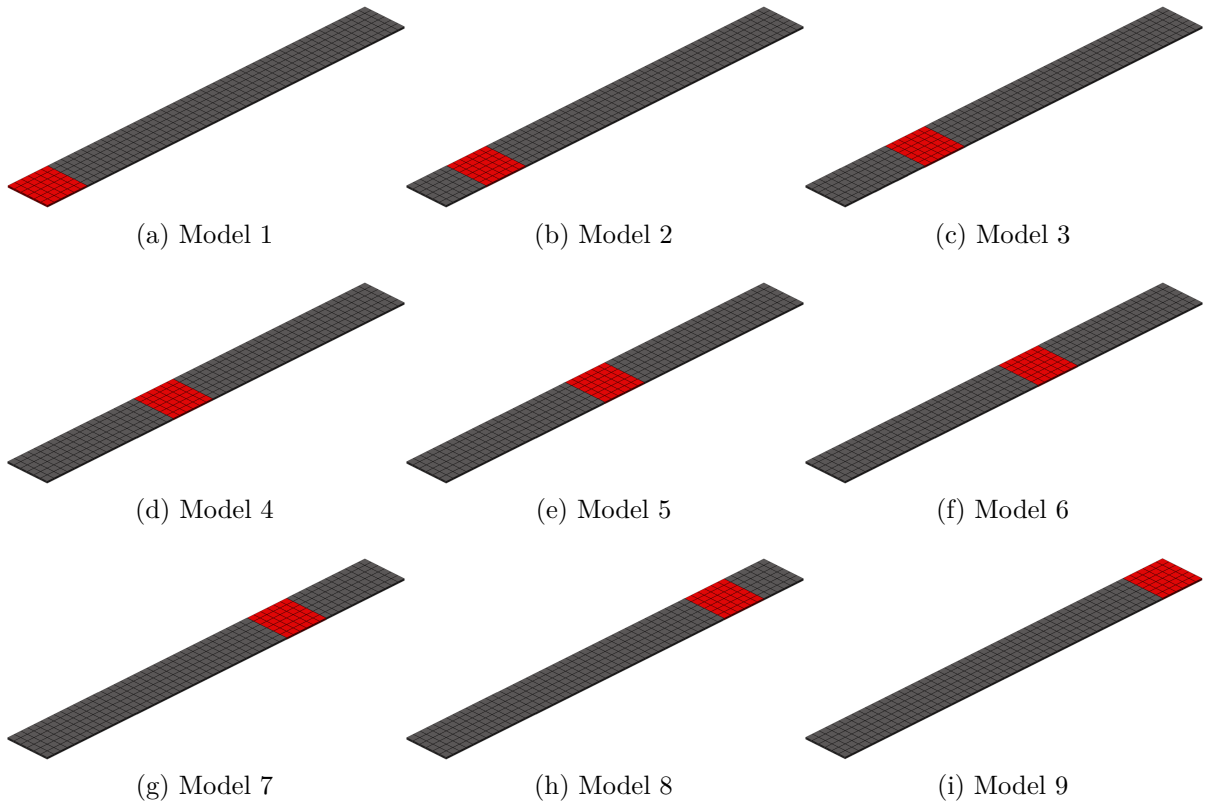


Figure 1 – Numerical models of a composite beam with nine different damage locations. The damage was modelled as a local stiffness reduction in a group of finite elements.

an issue since all data is obtained numerically. Figure 2 illustrates the Simplex-Lattice design used, for two combinations of components.

The flowchart in Figure 3 illustrates the main steps of the proposed methodology for tuning the damage index parameters.

Table 1 – Material properties of the composite material, used as inputs in the finite elements software for the laminated beam model.

Property	Value
$E_1$	116.62 GPa
$E_2$	5.40 GPa
$G_{12}$	5.00 GPa
$G_{13}$	5.00 GPa
$G_{23}$	2.24 GPa
$\nu_{12}$	0.20
$\rho$	1565 $kg/m^3$



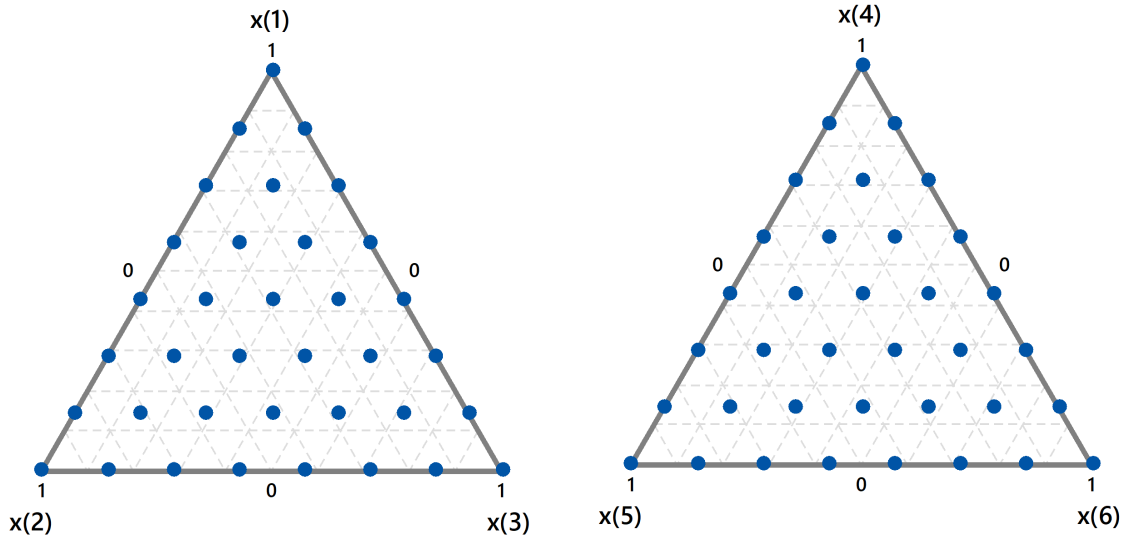


Figure 2 – Representation of the Simplex-Lattice Design used in the present study, for two combinations of the six components, with seven degrees.

## 2.3 Results and Discussion

### 2.3.1 Numerical Modal Analysis

Modal analysis was performed on the model using a Finite Element Analysis software, obtaining the first three mode shapes of the structure and their respective natural frequencies. Although it is possible to easily obtain more modes shapes in numerical analysis, only three modes were used in order to maintain the natural frequencies at lower values. In practical applications, modes shapes with higher frequencies have low amplitudes and are more affected by noise. Table 2 presents the mode shapes and natural frequencies of the pristine structure model and of a model with damage positioned in the center of the beam. For the damaged structure, the natural frequencies are shown for different levels of damage:  $\alpha = 0.1$ ,  $\alpha = 0.3$  and  $\alpha = 0.5$ .

Damage alters not only the natural frequencies of the structure but also their mode shape. However, the difference is not easily visible, hence the need for a damage index.

### 2.3.2 Damage Index

In order to identify damage in the laminated composite beam, a metric is proposed in this study. This metric is the damage index, composed of the detail coefficients generated by applying the DWT to mode shapes of the structure.

By the modal analysis, three mode shapes of the structure were obtained. Those

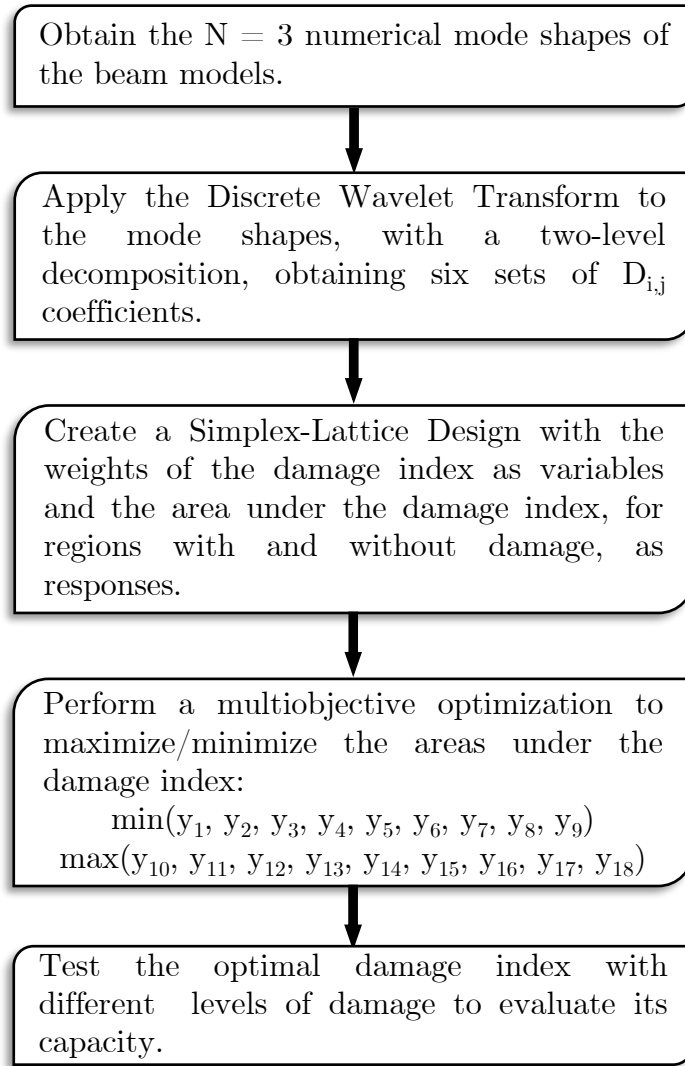


Figure 3 – Flowchart for the tuning process of the damage index components.


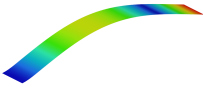
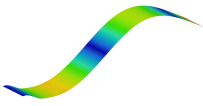
mode shapes were decomposed by DWT in two levels, resulting in six sets of detail coefficients. Two-level decomposition was chosen based on preliminary studies, decomposition at higher levels did not contribute significantly to the results. The *bi-orthogonal 3.1* (Figure 4) wavelet was used to decompose the signal. This mother wavelet was used by Vafaei *et al.* [36] and provided substantial results.

The proposed damage index (Eq. 2.8) consists in a weighted sum of the six detail coefficients obtained. For each  $D_{i,j}$  coefficient,  $i$  indicates the level of decomposition and  $j$  refers to the order of the mode shapes. The weights are denoted as  $w_i$ .

$$DI = w_1 \cdot D_{1,1} + w_2 \cdot D_{1,2} + w_3 \cdot D_{1,3} + w_4 \cdot D_{2,1} + w_5 \cdot D_{2,2} + w_6 \cdot D_{2,3} \quad (2.8)$$

The damage index without tuned weights is presented in Figure 5, the horizontal axis refers to the beam length in millimetres and the vertical axis is the value of the damage index. In this case, no tuning was done and each weight received the value of  $\frac{1}{6}$ , giving

Table 2 – Mode shapes and natural frequencies of a pristine and a damaged beam model with damage placed in the central position.

Mode	Shape	Pristine Structure $\omega_n$ [Hz]	Damaged Structure $\omega_n$ [Hz]		
			$\alpha = 0.1$	$\alpha = 0.3$	$\alpha = 0.5$
1st		20.435	16.772	19.285	19.920
2nd		128.023	83.282	105.837	116.334
3rd		358.503	337.601	352.873	356.063

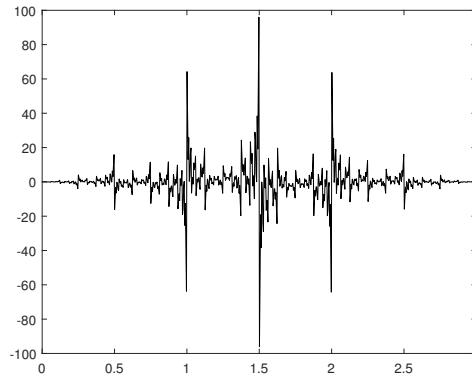


Figure 4 – Bi-orthogonal 3.1 wavelet, the mother wavelet chosen for obtaining detail coefficients of mode shapes.

the expected weight sum of 1. In the presence of damage, a disturbance in the form of a peak is expected in the damage index. However, there is little or no indication of damage presence using these weights. Therefore, it is important to assign appropriate weights to each component of the damage index, since each component contributes differently to the overall result of the index.

### 2.3.3 Mixture Design for Damage Index Tuning

For each combination of components generated in the Mixture Design, the damage index was plotted for nine beam models, encompassing all nine possible damage locations. The area under the damage index was calculated for each combination and the value divided between damaged regions and pristine regions.

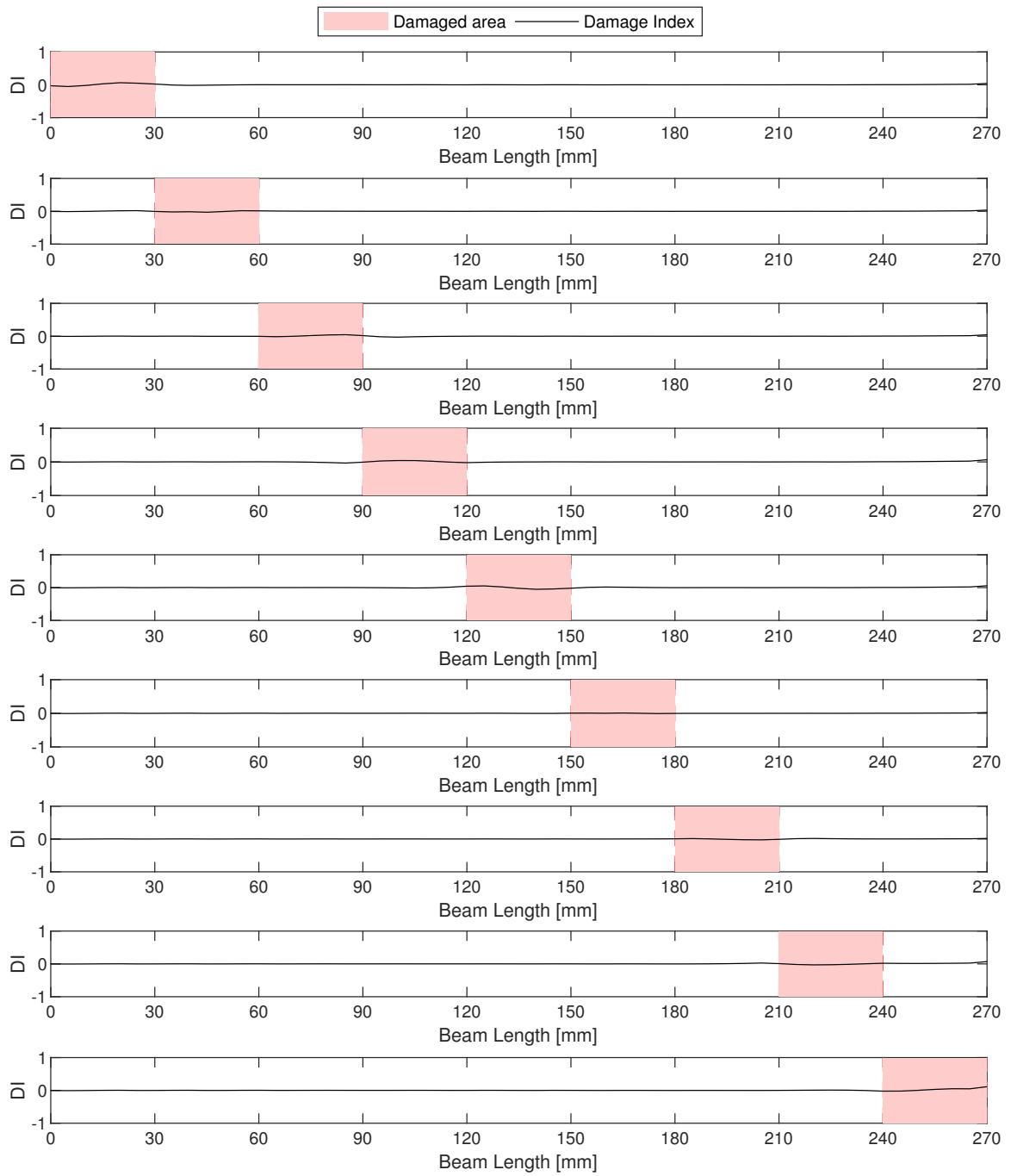


Figure 5 – Damage index without tuned parameters for a damage level of  $\alpha = 0.1$

Table 3 – Regression coefficients for the fitted regression model of the nine regions, with the presence of damage

	Region 1	Region 2	Region 3	Region 4	Region 5	Region 6	Region 7	Region 8	Region 9
$D_{1,1}$	0.0299	0.0308	0.0215	0.0371	0.0571	0.0680	0.0546	0.1003	0.6750
$D_{1,2}$	0.1792	0.3694	0.4173	0.2568	0.2064	0.3108	0.2716	0.3035	2.8280
$D_{1,3}$	1.3775	2.2330	0.6651	0.8219	1.5845	1.4867	0.8035	0.8288	9.9020
$D_{2,1}$	0.0448	0.4016	0.0903	0.2124	0.1056	0.2659	0.0622	0.1503	1.0550
$D_{2,2}$	1.9378	2.2483	3.9980	1.5151	1.4573	3.3538	1.7467	3.4180	7.2720
$D_{2,3}$	12.8514	3.0408	4.1752	8.2464	15.0616	1.5728	5.8198	11.2920	25.1740
$D_{1,1} \cdot D_{1,2}$						-0.2410			-3.1000
$D_{1,1} \cdot D_{1,3}$	-0.2935	-0.8830	-0.2709	-0.4200		-0.6520	-0.3990		-3.7100
$D_{1,1} \cdot D_{2,1}$				-0.1880					
$D_{1,1} \cdot D_{2,2}$	-0.3551	-0.4789	-0.4318	-0.3980	-0.6560	-1.6980	-0.7160	-1.8970	-3.9600
$D_{1,1} \cdot D_{2,3}$	-0.5513	-0.5077	-0.3225	-0.7140	-2.2340	-0.8500	-1.3270	-3.8880	-13.3200
$D_{1,2} \cdot D_{1,3}$	-0.1605	-0.4377	-0.1791	-0.5680	-0.7280	-1.4460	-1.0180	-1.1020	-16.7500
$D_{1,2} \cdot D_{2,1}$		-0.3396	-0.2497	-0.3320		-0.3280			
$D_{1,2} \cdot D_{2,2}$	-0.5080	-1.1082	-0.9211	-0.4380	-0.4920	-2.0230	-0.5010	-2.2780	-11.4000
$D_{1,2} \cdot D_{2,3}$	-0.7731	-1.0835	-0.6543	-1.5190	-2.6540	-1.3440	-1.9560	-4.0570	-8.0800
$D_{1,3} \cdot D_{2,1}$	-0.4503	-1.6030	-0.5561	-0.6820		-0.8810	-0.3500		-8.7300
$D_{1,3} \cdot D_{2,2}$	-1.4832	-3.8182	-1.6234	-1.3740	-2.5520	-4.0730	-2.7380	-2.8180	-4.4100
$D_{1,3} \cdot D_{2,3}$	-2.6526	-4.1004	-0.6888	-2.6500	-3.8010	-2.2500	-1.7180	-5.6110	-41.4900
$D_{2,1} \cdot D_{2,2}$	-0.6991	-0.1717	-0.7407	-1.6700	-1.0920	-3.4190	-0.9910	-2.3750	-9.1500
$D_{2,1} \cdot D_{2,3}$	-0.9783	-0.2390	-0.8298	-2.4480	-2.0590	-0.5080	-1.3000	-3.4330	-6.7400
$D_{2,2} \cdot D_{2,3}$			-0.7215	-0.2090	-10.6890	-6.9580	-7.0730	-22.0610	-45.1300

Table 4 – Regression coefficients for the fitted regression model of the nine regions, without the presence of damage

	Region 1	Region 2	Region 3	Region 4	Region 5	Region 6	Region 7	Region 8	Region 9
$D_{1,1}$	0.5600	0.6740	0.7390	0.7910	0.9430	0.9190	0.9150	0.7950	0.0511
$D_{1,2}$	2.6660	3.2870	2.7970	2.2950	2.6500	3.6570	5.0610	5.3740	0.1917
$D_{1,3}$	5.2620	5.8740	5.3900	6.5450	6.2060	4.3060	5.1990	10.1370	1.5590
$D_{2,1}$	1.2990	1.6380	1.8370	2.0260	2.4550	2.4610	2.1160	1.5240	0.0814
$D_{2,2}$	6.9920	9.4440	9.6300	6.8040	8.7170	11.2750	15.2090	15.2130	1.0488
$D_{2,3}$	17.6670	16.5130	17.7430	20.6250	23.7780	13.0330	19.0100	30.5970	6.9707
$D_{1,1} \cdot D_{1,2}$	-3.1020	-3.6990	-3.6660	-3.2960	-3.9590	-5.2390	-6.0660	-5.3600	
$D_{1,1} \cdot D_{1,3}$	-2.0120	-2.1030	-1.9440	-2.0550	-1.7640	-1.1450	-1.5970	-4.0600	-0.5860
$D_{1,1} \cdot D_{2,1}$	-1.0440	-1.2960	-1.7800	-2.1390	-2.5040	-2.7240	-1.9530		
$D_{1,1} \cdot D_{2,2}$	-3.9680	-4.7110	-4.5590	-3.3030	-4.6500	-6.0290	-8.3230	-8.7100	-0.2690
$D_{1,1} \cdot D_{2,3}$	-8.5790	-8.6660	-9.2160	-9.8470	-11.6660	-8.7040	-11.3680	-16.3000	-1.2180
$D_{1,2} \cdot D_{1,3}$	-11.7060	-12.4370	-11.7060	-10.8400	-11.1900	-11.6920	-15.9840	-23.2200	-0.9950
$D_{1,2} \cdot D_{2,1}$	-1.3350	-1.6040	-1.4790	-1.4700	-1.4430	-2.1240	-2.3170	-2.4000	
$D_{1,2} \cdot D_{2,2}$	-11.0130	-13.2120	-12.0010	-8.7350	-11.3080	-15.5000	-22.4060	-22.1900	-0.4400
$D_{1,2} \cdot D_{2,3}$	-5.5240	-5.6810	-5.9890	-5.4550	-7.7670	-5.6500	-8.1160	-12.6100	-1.5060
$D_{1,3} \cdot D_{2,1}$	-5.8130	-6.6030	-7.0210	-8.4970	-8.3000	-6.8660	-6.9690	-9.2800	-0.6030
$D_{1,3} \cdot D_{2,2}$	-4.2170	-6.0650	-5.3540	-4.1100	-5.6090	-7.2250	-8.5090	-10.9300	-1.6560
$D_{1,3} \cdot D_{2,3}$	-22.3120	-22.5750	-22.1180	-25.5330	-26.9050	-17.2170	-22.1850	-40.7900	-4.5840
$D_{2,1} \cdot D_{2,2}$	-9.4480	-11.0350	-12.4890	-11.3270	-14.5360	-17.8850	-19.4840	-16.4300	-0.2760
$D_{2,1} \cdot D_{2,3}$	-5.2000	-3.4680	-4.9330	-4.0760	-4.5460	-2.1140	-4.5060	-9.0800	-1.3590
$D_{2,2} \cdot D_{2,3}$	-33.8570	-35.5600	-34.5350	-30.0060	-42.1620	-38.2070	-57.5440	-74.2900	-3.4350

This resulted in eighteen responses for the mixture design: Nine values of area for regions with damage and nine for regions where there was not damage. With these responses, the MD generated regression coefficients exhibited in Tables 3 and 4.

Some statistics are used to evaluate the quality of the regression models. These statistics are presented in Table 5 for all responses, where  $S$  is the standard deviation of

Table 5 – Model summary table for the fitted regression model.

Response	$S$	$R^2$	$R^2 (adj.)$
Region 1 - With Damage	0.0678	99.92%	99.91%
Region 2 - With Damage	0.0550	98.85%	98.83%
Region 3 - With Damage	0.0402	99.80%	99.79%
Region 4 - With Damage	0.0779	99.71%	99.70%
Region 5 - With Damage	0.2195	99.24%	99.22%
Region 6 - With Damage	0.0910	94.68%	94.55%
Region 7 - With Damage	0.1321	97.80%	97.75%
Region 8 - With Damage	0.3518	95.18%	95.08%
Region 9 - With Damage	0.7861	94.17%	94.04%
Region 1 - No Damage	0.4400	96.40%	96.31%
Region 2 - No Damage	0.4344	95.86%	95.76%
Region 3 - No Damage	0.4244	96.68%	96.59%
Region 4 - No Damage	0.4751	97.13%	97.06%
Region 5 - No Damage	0.5847	96.63%	96.54%
Region 6 - No Damage	0.3958	95.07%	94.94%
Region 7 - No Damage	0.5777	94.97%	94.85%
Region 8 - No Damage	0.9147	94.52%	94.39%
Region 9 - No Damage	0.0798	99.48%	99.47%

the sample,  $R^2$  represents how much the variation in responses are explained by the model and the  $R^2 (adj.)$  is the adjusted version of  $R^2$  which takes into account the number of predictors in relation to the number of observations. The  $R^2 (adj.)$  of all responses are high, with minimum value of 94%.

The results of the MD can be visualized using a ternary plot. This plot displays the relationship between the components (three at a time) for each response. Figures 6 and 7 presents the ternary plots for two component combinations:  $D_{1,1} - D_{1,2} - D_{1,3}$  and  $D_{2,1} - D_{2,2} - D_{2,3}$ . In the plot, the blue color corresponds to lower values of the response while the yellow color corresponds to the higher values.

### 2.3.4 Optimization Results

The mixture design analysis generated regressions for the areas that contain and do not contain damage, these regressions are the objective functions and are presented in the A. To optimize the weights of the damage index, the equations for areas that contain damage must be maximized while the areas that do not contain damage must be minimized.

There are eighteen objective functions in total, therefore this is a multiobjective optimization problem. The algorithm selected for this optimization is the NSGA-II (Non-dominated Sorting Genetic Algorithm II) [41]. The algorithm was executed with the following parameters: population size of 600, mutation defined by a Gaussian distribution

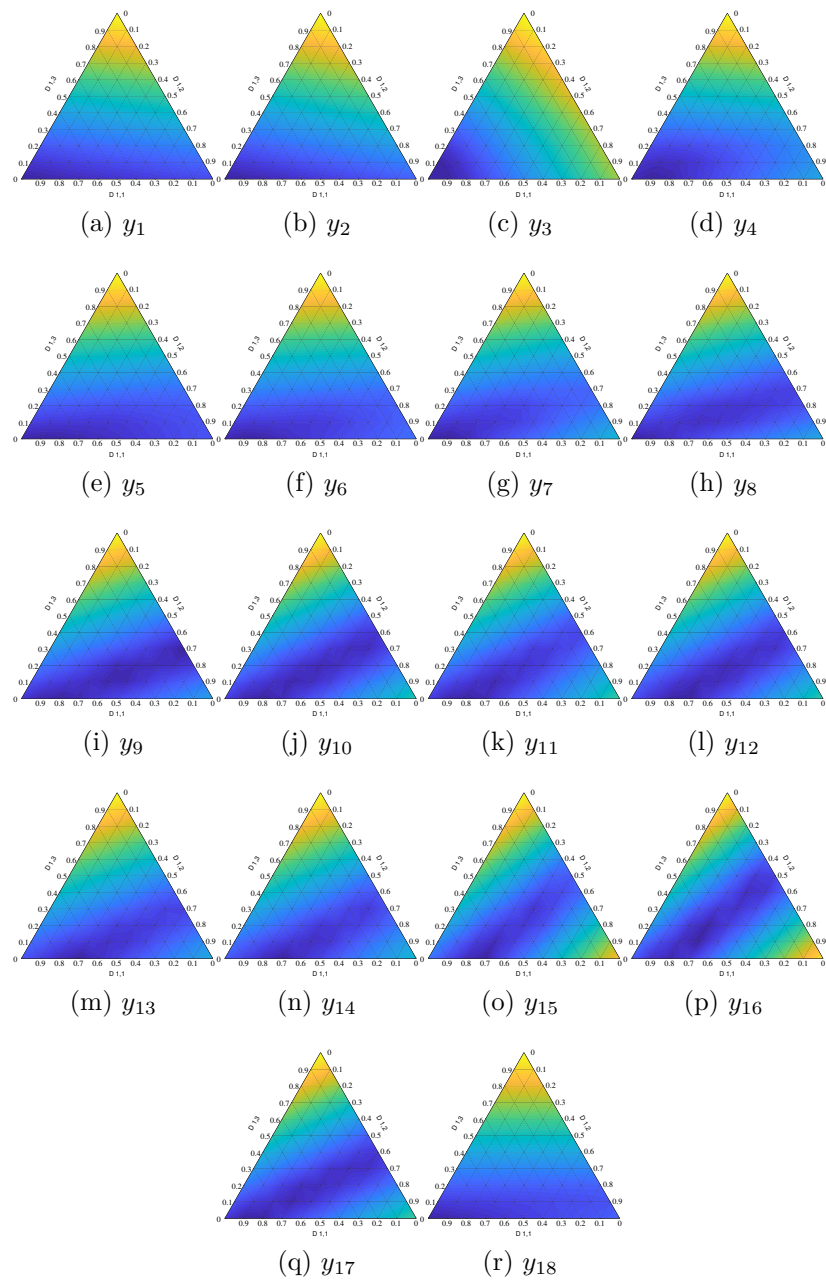


Figure 6 – Results of the simplex-lattice design for damage index parameter tuning. Plotted for the components  $D_{1,1} - D_{1,2} - D_{1,3}$ .

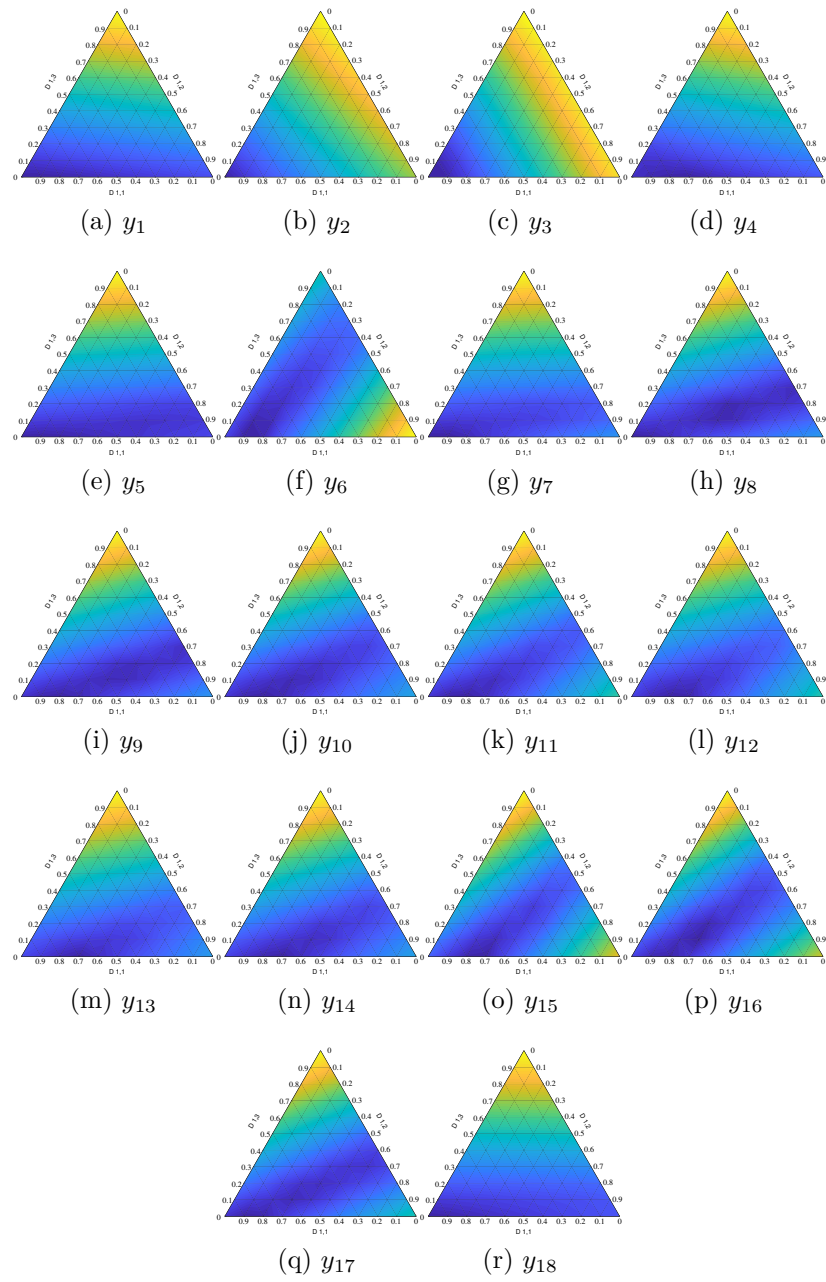


Figure 7 – Results of the simplex-lattice design for damage index parameter tuning. Plotted for the components  $D_{2,1} - D_{2,2} - D_{2,3}$ .



and 1000 as the maximum number of generations. Figure 8 contains the performance plots of the optimization. Figure 8a is the histogram for the scores of the eighteen objective functions. Figure 8b and Figure 8c exhibits the fitness for each individual and the average distance between individuals through the generations, both graphs indicate a good amount of diversity which is good for convergence and coverage in multiobjective optimizations. Figure 8d and Figure 8e presents the distance and spread of the individuals, the spread acquires small values when the extreme objective function values do not change much through generations and when the Pareto front points are evenly spread, this determine the stopping condition.

The optimum solution was selected from the Pareto Front, presented in Figure 9 for three responses at a time, using the Technique for Order Preference by Similarity to Ideal Solution (TOPSIS) [42]. Eq. 2.9 presents the proposed damage index with tuned weights, obtained by the optimization.

$$DI = 0.040 \cdot D_{1,1} + 0.106 \cdot D_{1,2} + 0.025 \cdot D_{1,3} + 0.010 \cdot D_{2,1} + 0.001 \cdot D_{2,2} + 0.818 \cdot D_{2,3} \quad (2.9)$$

The damage index with tuned parameters yielded substantial results. In Figure 10, the presented DI refers to beam models with damage level of  $\alpha = 0.1$ . There is a clear disturbance in the DI for almost all damage positions, unlike what occurred when the weights were not calibrated. The peak in the DI at the free end of the beam occurs because the DWT is the product of a wavelet function and a signal of infinite length, however, mode shapes are a finite length signal which causes a distortion at the border. This peak affects damage identification at the free end of the beam.

The damage identifying capacity of the index is further investigated for other damage levels. Figure 11 presents the results for beam models with damage level of  $\alpha = 0.3$  and, although the disturbances have a lower amplitude, they are still visible. For beam models with damage level of  $\alpha = 0.5$ , exhibited in Figure 12, the disturbance in DI is indistinguishable, thus  $\alpha = 0.3$  is the limit in stiffness reduction for damage identification using the proposed method.

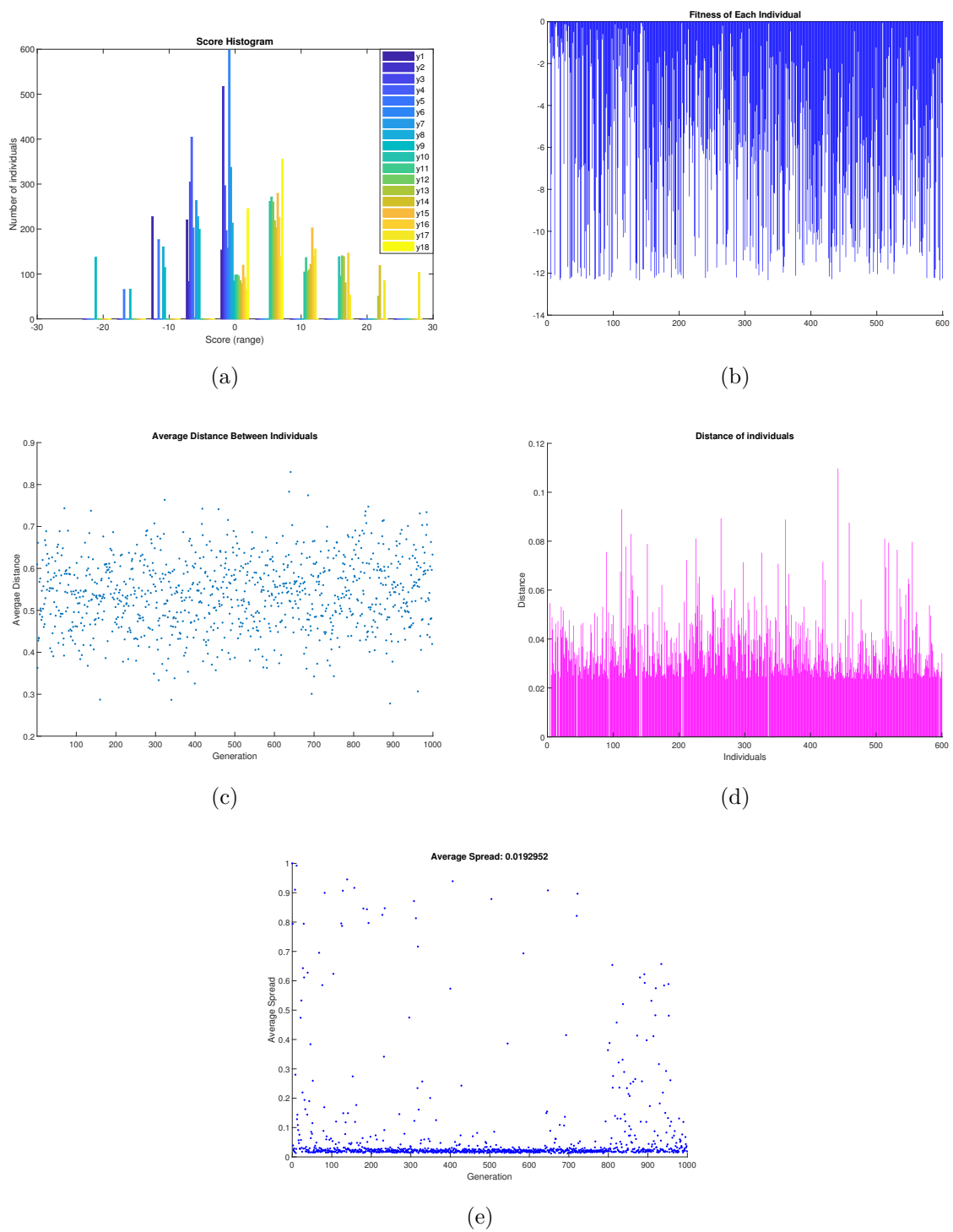


Figure 8 – Performance plots for the optimization performed with NSGA-II.

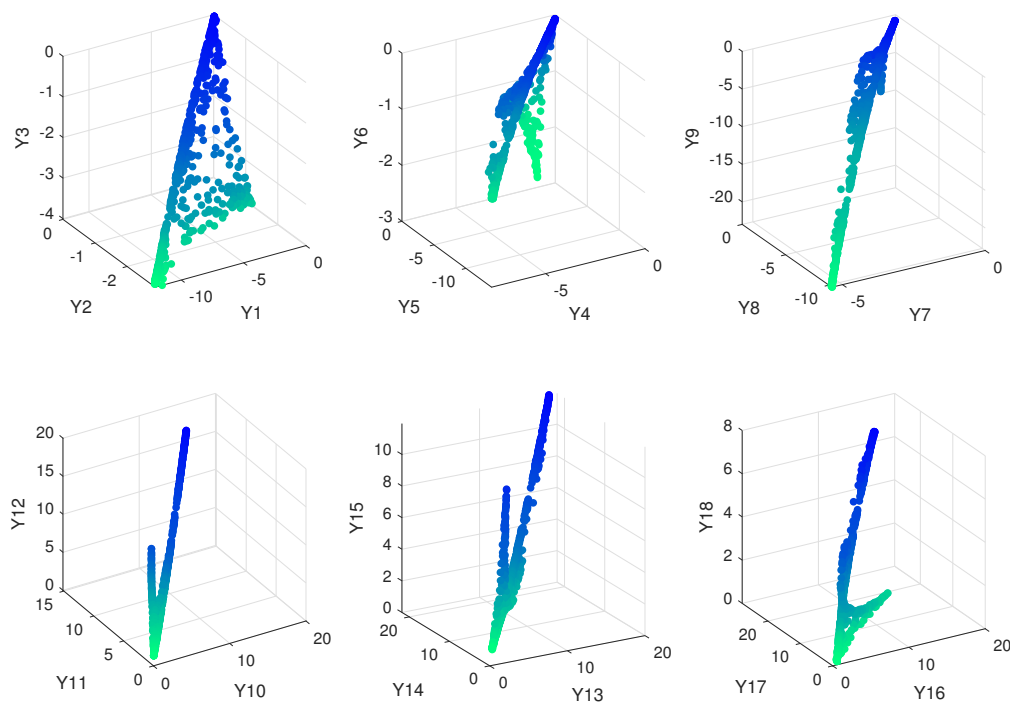


Figure 9 – Pareto Front represented for three responses at a time.

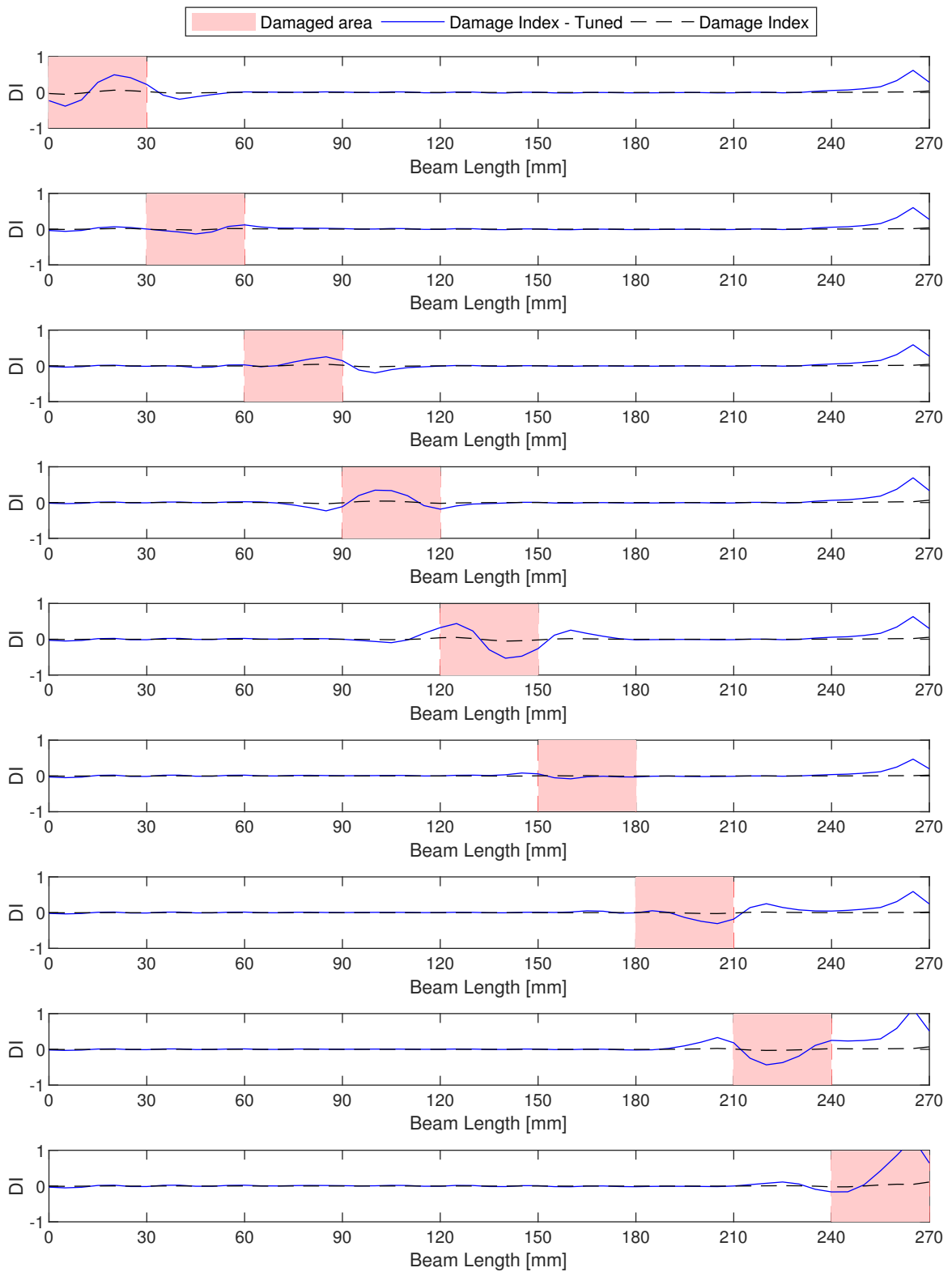
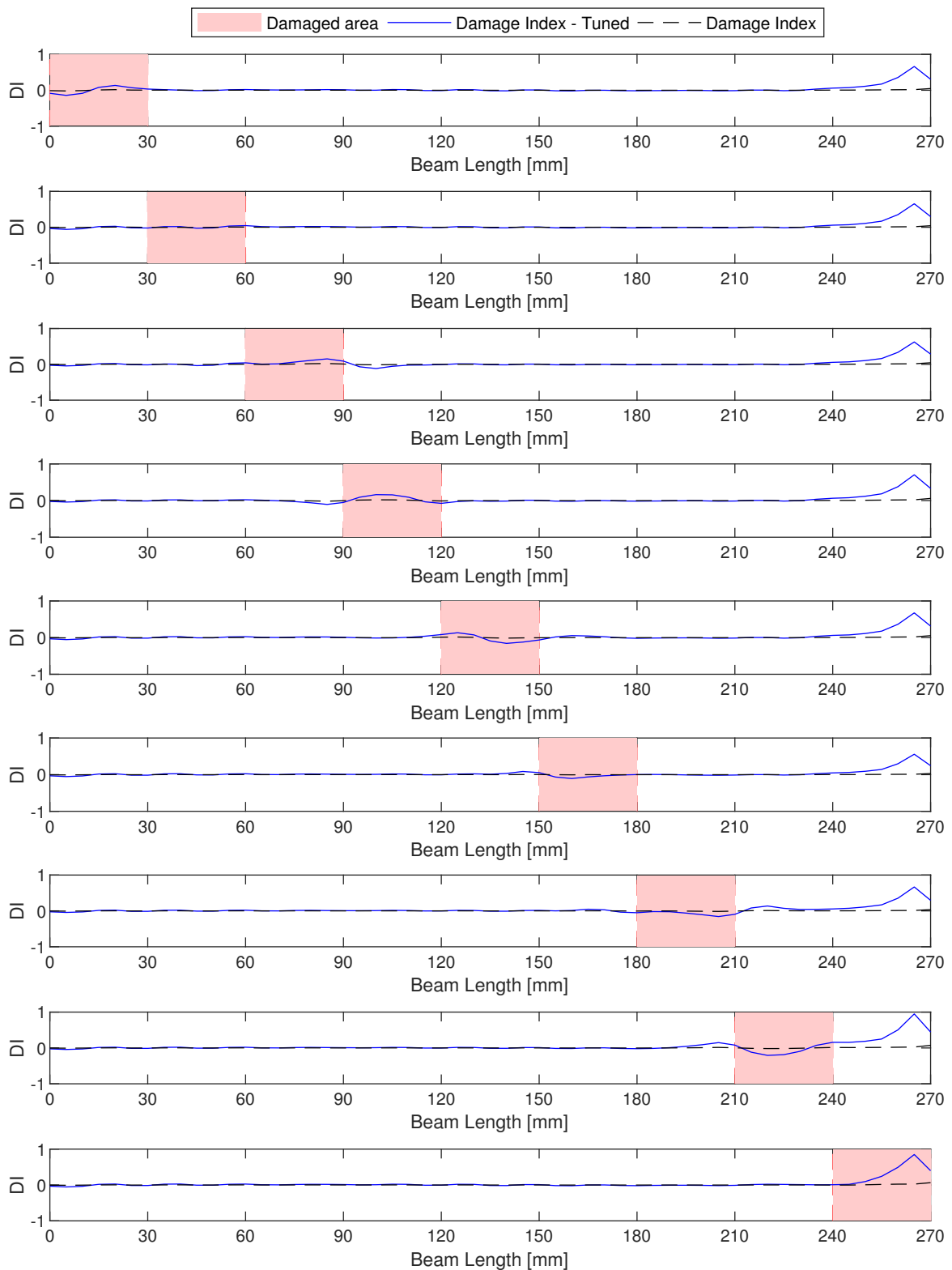


Figure 10 – Damage index with tuned parameters for a damage level of  $\alpha = 0.1$

Figure 11 – Damage index with tuned parameters for a damage level of  $\alpha = 0.3$

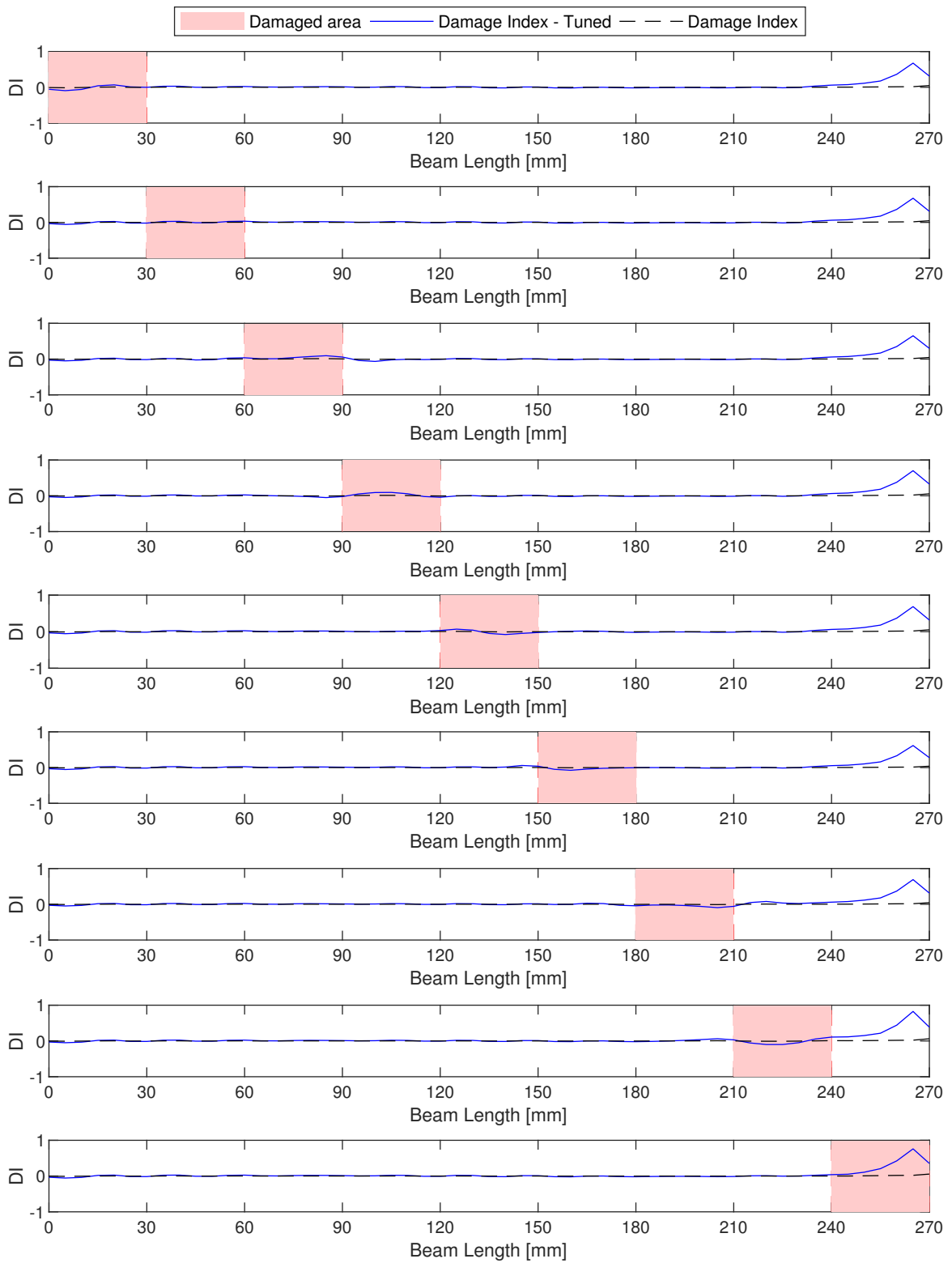


Figure 12 – Damage index with tuned parameters for a damage level of  $\alpha = 0.5$

## 2.4 Conclusion

In this chapter, a damage index to identify delaminations in a laminated composite beam was proposed. To improve the performance of the damage index, its parameters were tuned using a mixture design analysis and a multiobjective optimization. The damage index achieved a solid performance, it pinpointed the correct damage location in all positions. The extent of the damage identification capacity was also tested and the index provided substantial results up to a reduction in stiffness of 30%.

The damage index produced an undesired peak at the free end of the beam due to the discontinuity of signal, which causes a distortion in the wavelet coefficients. However, the overall results are a noteworthy contribution as the proposed method is no-baseline, meaning it does not require information of the pristine structure.

# 3 Experimental Damage Identification in Laminated Composite Beams

In the previous chapter, the development of the damage index was presented along with tests of its efficiency in numerical scenarios. However, in real situations, obtaining mode shapes is subject to problems such as noise. Thus, it is necessary to test the effectiveness of the index in experimental scenarios. For this, real beam specimens made of CFRP were produced with delaminations induced by embedding non-sticking films between the layers.

These specimens were subjected to experimental modal analysis to obtain mode shapes and to DIC to obtain the strain fields. Both acquired data were used in an attempt to identify the damage and the results of these tests are presented in this chapter.

The chapter is organized as follows: Section 3.1 provides the theoretical background on the topics of mode-shape-based damage identification and digital image correlation. Section 3.2 presents the experimental methodology used for producing the laminate composite beam specimens and for performing the modal testing. Section 3.3 presents the results of the experimental modal analysis followed by the results of the damage identification using mode shapes. This section also presents the attempt to identify damage in the beams through the strain fields obtained with the digital image correlation technique. Finally, in Section 3.4 the conclusions are drawn.

## 3.1 Theoretical Background

### 3.1.1 Mode Shape-based Damage Identification

The present study uses mode shapes as basis for damage identification. This dynamic characteristic of a structure can be obtained through numerical or experimental techniques. Modal analysis in a numerical model consists on solving Eq. 3.1, where  $K$  and  $M$  are respectively the stiffness matrix and the mass matrix of the structure.

$$[K - \lambda \cdot M] \phi = 0 \quad (3.1)$$

The solution of this equation provides the eigenvalues ( $\lambda$ ), which represent the natural frequencies squared. For each eigenvalue is obtained a eigenvector  $\Phi$ , which represents the mode shapes, the deformed shapes the vibrating structure will acquire while at the natural frequency [43].



For an experimental modal analysis, the natural frequencies and mode shapes are obtained from the frequency response function, which is a function that establishes the relationship between the excitation and the vibrational response of the structure [44]. Although natural frequencies can be successfully used as inputs in damage identification, as done by Oliver *et al.* [45], mode shapes are more robust sources.

Mode shapes are excellent and extensively used metrics for identifying damage. Several studies using mode shapes for damage identification have been published. Rucevskis *et al.* [46] used a mode shape curvature-based method to identify damage in plate-like structures with the advantage of using only information from the damaged state of the structure. Ciambella *et al.* [47] obtained precise damage localization by filtering the modal curvature variation between damaged and pristine structures. Ghannadi *et al.* [26] formulated the damage identification as an optimization problem, and verified that the objective function based only on natural frequencies was not sensitive enough for identification yet obtained effective results by adding modal shapes to the objective function. Gomes *et al.* [48, 49] developed damage identification methods using vibrational data and optimization algorithms both in a simple plate structure and in a complex structure, a helicopter main rotor blade.

### 3.1.2 Digital Image Correlation

The Digital Image Correlation method has been widely used as a robust tool for measuring fields of displacements and strains in the area of experimental solid mechanics [50]. It consists in analysing the surface of a structure by recording digital images of the specimen while it is being deformed. The software for post-processing makes the correlation for the position of all pixels that compose the image, determining its path during the experiment.

The setup is simple, requiring only a fixed charge-coupled device (CCD) camera to record the digital images and a computer for post-processing data. The only requirement for the test specimen is that its surface must have a random high contrast speckle pattern, which can be obtained by spraying paint.

Compared to conventional methods such strain gauges, DIC can investigate a larger area and has the advantage of being a contactless method.

## 3.2 Experimental Methodology

In order to validate the proposed damage index to identify delaminations, nine carbon fiber-reinforced polymer (CRFP) beams were manufactured, one intact and the other eight with delaminations in different locations according to Figure 13.

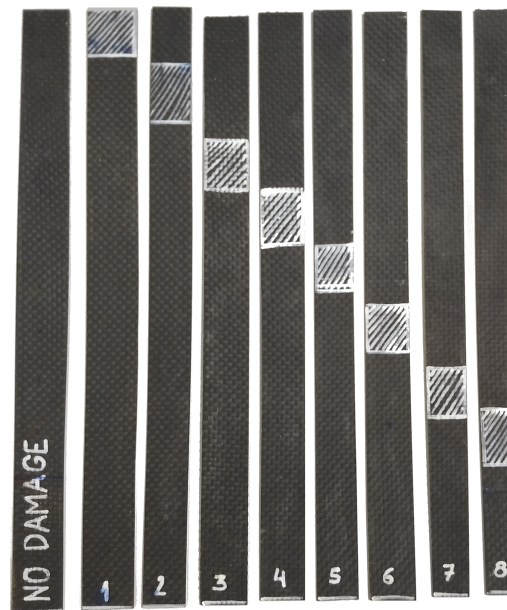


Figure 13 – CRFP laminated beam specimens, one intact and eight with induced delaminations in different longitudinal positions.

The CFRP beams were fabricated as the numeric model presented in Section 2.2.1, constituted of 4 layers with thickness of 0.3 mm each, all layers oriented at  $0^\circ$ . The delamination was induced by embedding Teflon films, which were removed after manufacturing and can be seen in Figure 14.

The modal testing setup was composed of a Laser Doppler Vibrometer (Ometron<sup>®</sup>) to capture the vibration data of ten points, an impact hammer (Brüel & Kjær<sup>®</sup>, Type 8204) to excite the laminated beam and a dynamic signal analyzer (Brüel & Kjær<sup>®</sup>, Photon+) for data acquisition and post-processing. All equipments are shown in Figure 15a. To ensure no movement on one end of the beam, the support shown in Figure 15b was used.

Performing modal testing using a Laser Doppler Vibrometer has the advantage of a non-contact approach: not adding mass to the analyzed structure, which is important when the structure is light. However, a rough or dark surface can affect the laser reflection. To enhance the reflectiveness, white tags were affixed to the surface of the laminate in the ten points of measurement, as seen in Figure 15b.

After modal testing, the specimens were subjected to a tensile stress below their yield strength, by a universal test machine (INSTRON<sup>®</sup>, Model 8801). The strains generated in this test were acquired by a charge-coupled device camera.

The data acquisition system requires a high contrast and random pattern imprinted in the test subject. Since the specimens are dark, white paint was sprayed along one face of the beam using a brush, creating the desired pattern. The collected data was processed using INSTRON Bluehill<sup>®</sup> software.

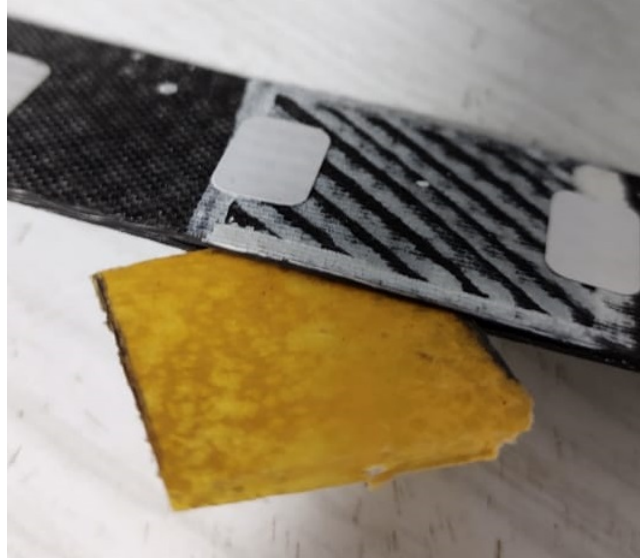


Figure 14 – Teflon film used to induce delamination being removed after the laminate manufacturing.

## 3.3 Results and Discussion

### 3.3.1 Experimental Results

From the modal testing performed in the beam specimens, the natural frequencies (Table 6) and mode shapes were obtained for the first three modes. The Laser Doppler Vibrometer acquired the response in velocity through time and the dynamic signal analyzer converted the response to the frequency domain. The imaginary component of the frequency response function has peaks above or below zero which indicate the natural frequencies. With the peaks of several measurements along the structure the mode shapes can be determined.

Measurements were taken in ten different points of the beam, which were sufficient for obtaining the mode shapes. However, to apply the wavelet transform and obtain its coefficients for the damage index, more points are needed. A cubic spline interpolation was used for obtaining extra points for the wavelet transform. The results of the interpolation for one of the beam specimens is shown in Figure 16.

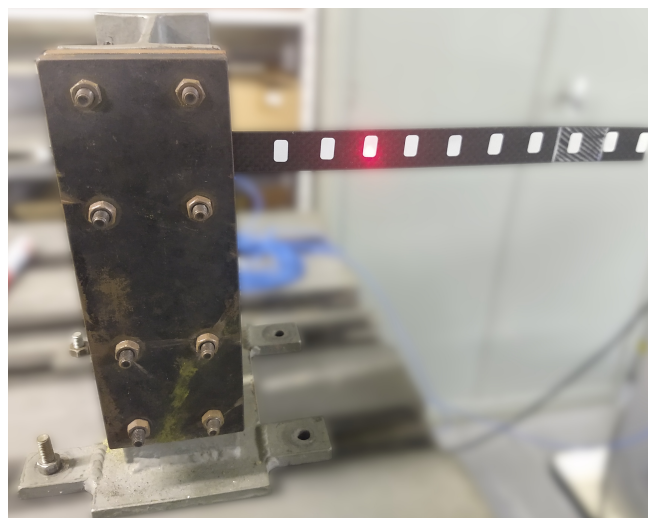
### 3.3.2 Damage Identification for Mode Shapes

The damage index presented in Section 2.3.4 was applied for both numerical and experimental data. The DI for the eight beams fabricated with delaminations is presented in Figure 17. The location of the delamination, determined by the disturbance in the DI, is clear in all cases. The only exception is when the delamination is at the free end of the beam, due to the distortion caused by using a finite length signal.

There is a spike in the DI at the free end of the beam in some cases. This occurs



(a) Equipments used for modal testing.

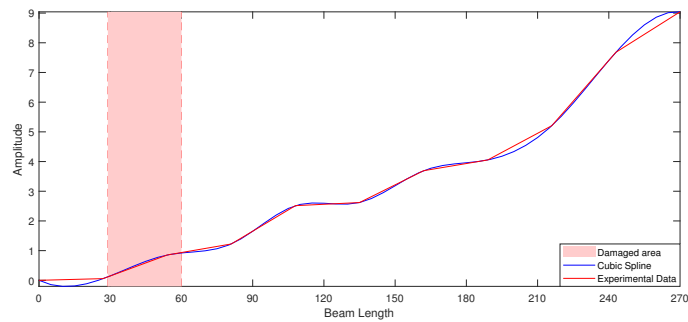


(b) Support used for fixing one end of the beam, ensuring no movement.

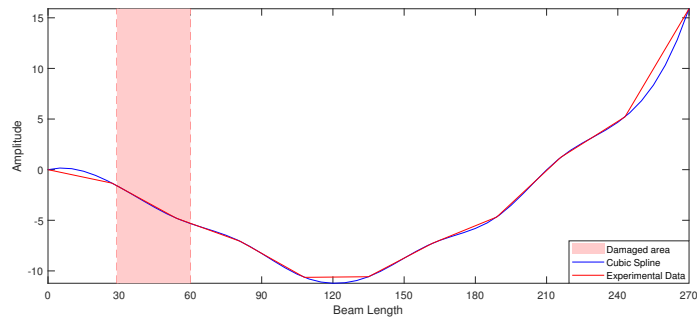
Figure 15 – Experimental setup for the modal testing.

Table 6 – Natural frequencies of the beam specimens, in Hertz.

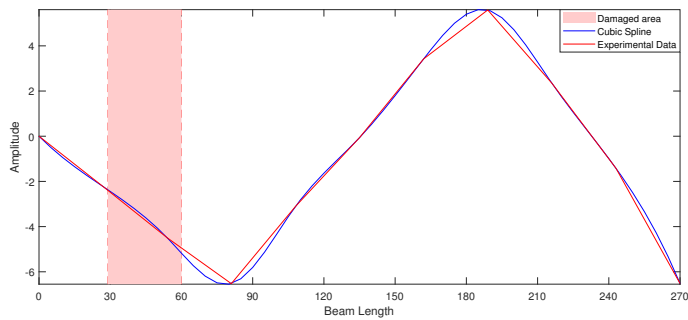
Specimen	$\omega_1$	$\omega_2$	$\omega_3$
1	16.25	101.50	278.50
2	15.00	97.75	280.00
3	15.00	95.50	275.00
4	15.75	104.00	262.25
5	15.25	99.00	263.25
6	16.00	98.75	284.50
7	16.50	93.00	266.50
8	17.75	103.75	264.75
No Damage	14.50	91.50	255.00



(a) First mode shape.



(b) Second mode shape.



(c) Third mode shape.

Figure 16 – Comparison between the experimental mode shapes and their respective cubic spline approximation.

because the DWT is the product of a wavelet function and a signal of infinite length, as seen in Section 2.1.1. However, the mode shapes are a finite length signal and this causes a distortion at the border.

### **3.3.3 Damage Identification for Strain Fields**

The procedure using the DIC technique, explained in Section 3.2, was done to four specimens of the beam. After post-processing the acquired data, strain fields were obtained and are presented in Figure 18. It can be observed that composite materials have a complex configuration of strains.

Discrete Wavelet Transform was applied to the strain fields using the bi-orthogonal 3.1 mother wavelet. Since the image has two dimensions, the wavelet followed three paths: the horizontal axis, the vertical axis and a diagonal path. For each path, detail coefficients were generated and a approximation of the original image is created. Figure 19 exhibits the wavelet coefficients of approximation and detail, the colors of the plot were adjusted for better visualization.

No indication of damage was observed after applying the DWT. The complexity of strain fields in composite materials and the fact that delamination is an internal damage might hinder the identification of damage in this method.

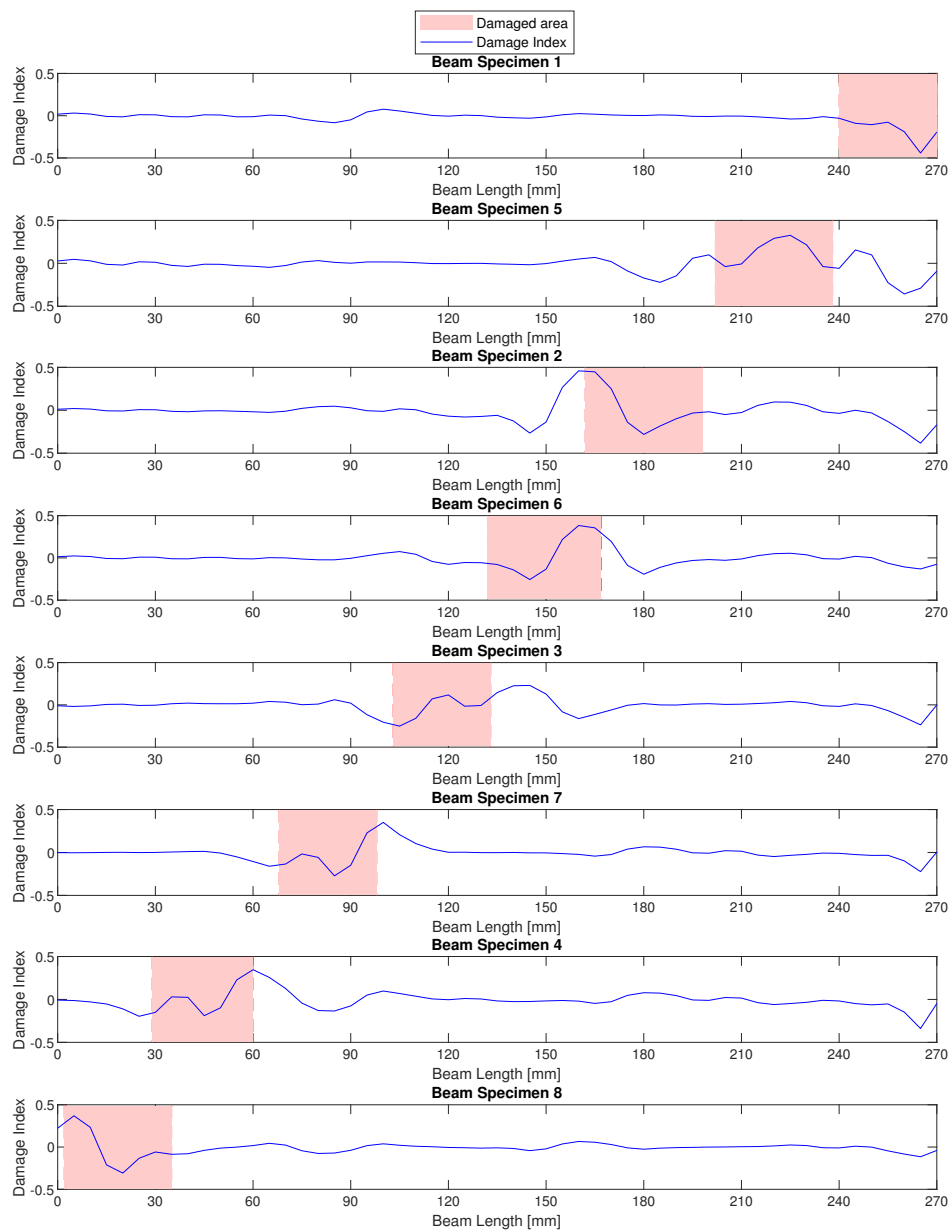


Figure 17 – Damage index of the eight beams considering induced delamination in different positions.

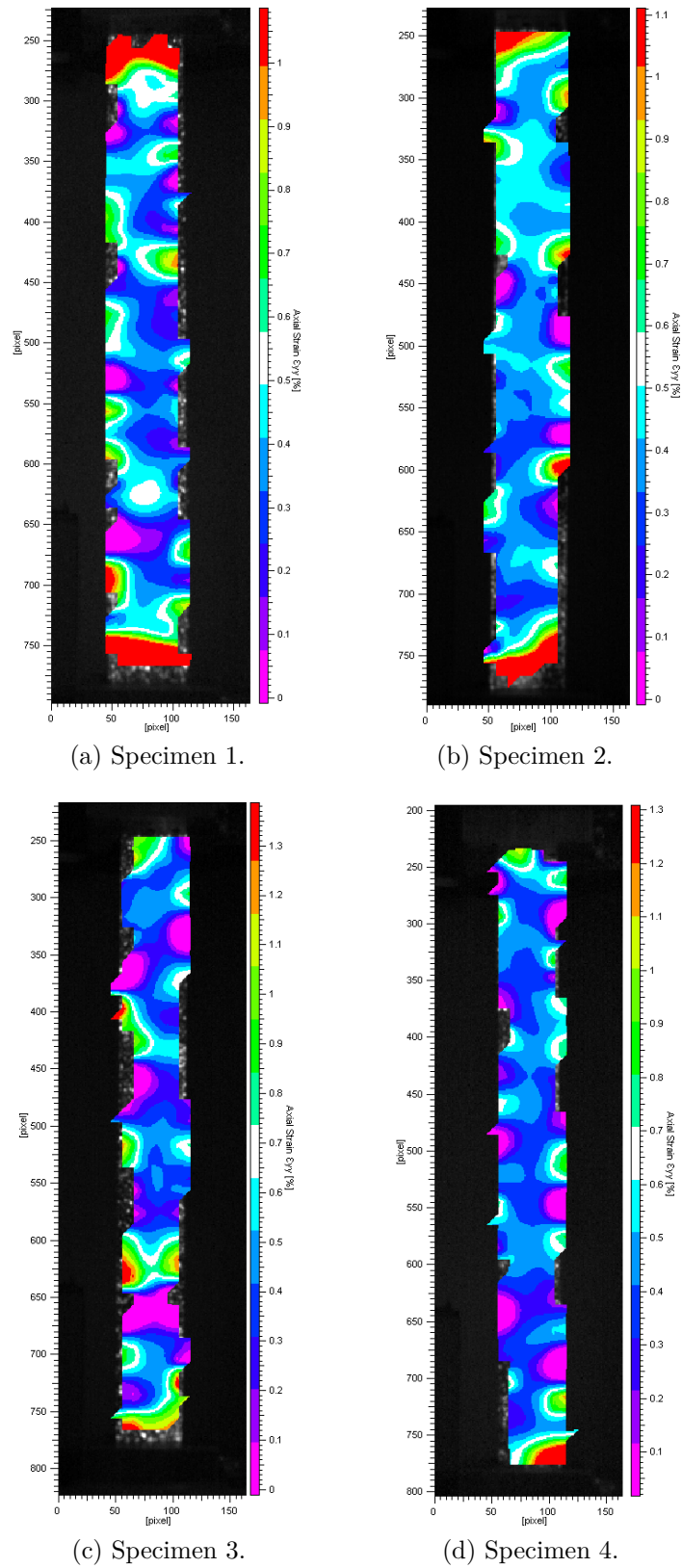


Figure 18 – Strain fields obtained by Digital Image Correlation.



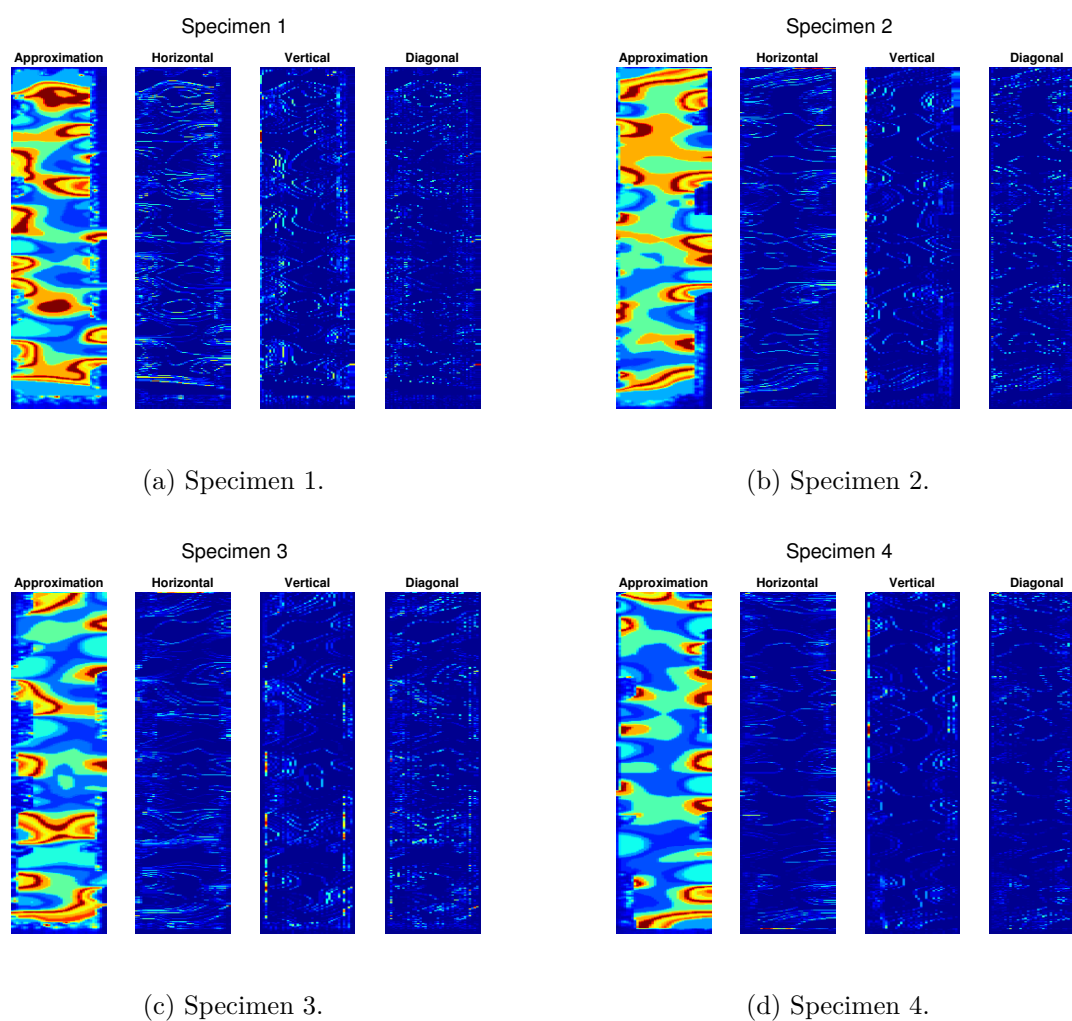


Figure 19 – Coefficients of the Wavelet Transform applied to strain fields obtained by Digital Image Correlation.

## 3.4 Conclusion

In this chapter, the proposed damage index was tested in experimental specimens. The performance of the index was extremely satisfactory as it correctly pointed the damage location in almost all positions. It was noticed an issue with damages placed in the free end of the beam: Due to the discontinuity of signal the wavelet coefficients suffer a distortion. Nevertheless, the proposed methodology worked well for the specific structure discussed and serves as basis for further investigations to more generic structures. The Wavelet-based damage identification using strain fields presented in this chapter did not yield good results. However, this attempt, which is the first of its category, may provide information for future endeavours in the area.

# 4 Statistical Analysis In Damage Identification Using Wavelet Transform

## 4.1 Introduction

The proposed damage index yielded substantial results in both numerical and experimental scenarios, as presented in Chapters 2 and 3. To better understand the capabilities of the damage index and how the characteristics of the damage affect the efficiency, a statistical analysis of the damage identification problem using techniques as ANOVA and RSM is done and presented in this chapter.

The chapter is organized as follows: Section 4.2 provides the theoretical background on the topic of response surface method. Section 4.3 presents the validation of the numerical-experimental methodology by comparing the dynamic characteristics of models and specimens along with a statistical analysis of how the parameters of the damage influence the overall identification response. Finally, in Section 4.4 the conclusions are drawn.

## 4.2 Theoretical Background

### 4.2.1 Response Surface Method

The Response Surface Method (RSM) is a stepwise heuristic that uses first-order polynomials as inputs and as the method approaches the optimum, the latest first-order polynomial is replaced by second-order polynomial which allows the estimation of the optimum [51]. This statistical technique generates a surface that describes the relation of the factors to a determined response. According to [38], the second-order model in Equation 4.1 is adequate for most cases that require a curvature to approximate the response. In this model,  $k$  represents the number of design parameters and  $\beta$  represents the coefficients to be determined.

$$Y = \beta_0 + \sum_{i=1}^k \beta_i x_i + \sum_{i=1}^k \beta_{ii} x_i^2 + \sum_{i < j} \beta_{ij} x_i x_j + \varepsilon \quad (4.1)$$

There are several types of designs to fit a response surface, each with its particular advantages or disadvantages. For the present study, the Central Composite Design (CCD) was chosen for modeling. The model is constructed with a complete or fractional  $2^k$

Table 7 – CCD design with the input parameters and respective levels.

Parameter	Nomenclature	Unit	Level		
			-1	0	+1
Damage Position	$x_1$	[m]	0	0.12	0.24
Severity	$x_2$	-	0.1	0.5	0.9

factorial layout, plus  $2k$  axial points along the coordinate axes and an observation at the design center [37].

The three main characteristics of the damage index illustrated in Figure 20 will be used as responses in the RSM: The blue area encompasses the area where damage is present, therefore it must be maximized. The red area encompasses the area where damage is not present, therefore it represents false positives and must be minimized. Finally, the green dot represents the peak value of the DI and ideally it must be at the center of the damaged area.

The factors which may influence in the responses are the damage location and the damage severity level. The CCD design for this study with the parameters and their respective values is presented in Table 7.

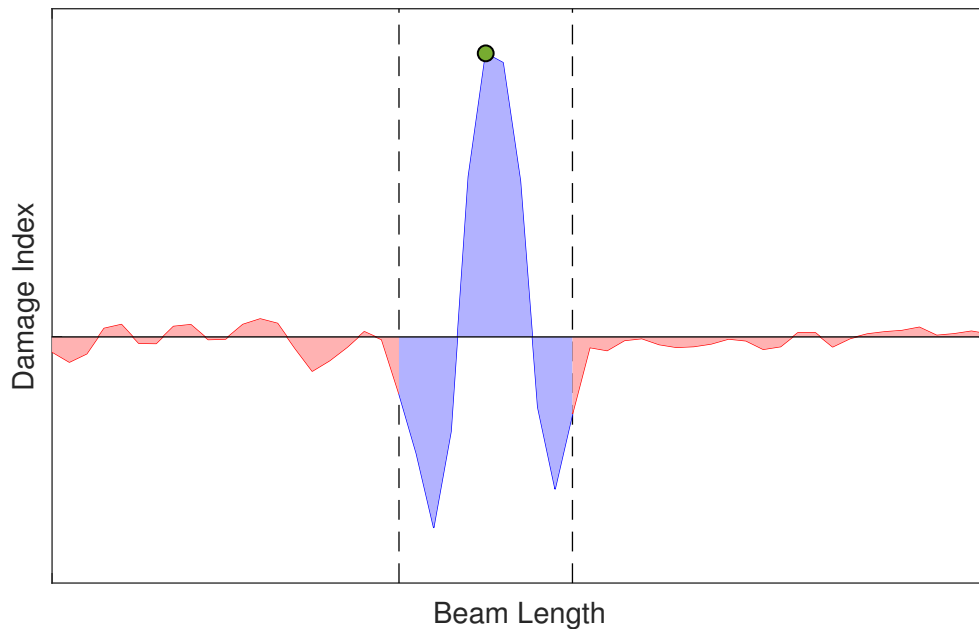


Figure 20 – Illustration of the damage index behavior. The blue area encompasses the area where damage is present, the red area indicates false-positives and the green dot is the peak value of the DI.

## 4.3 Results and Discussion

### 4.3.1 Numerical-Experimental Validation

The numerical models were created using the mechanical properties of Table 1 (from Section 2.2.1) and used a stiffness reduction in a group of elements to simulate damage. This approach allows the damage to be easily modelled with different levels of severity. However, it is necessary to test the validity of this methodology by comparing the natural frequencies and mode shapes of numerical models and real CFRP specimens.

The CFRP laminated beams were fabricated with the same layup of the numerical models. The damage, a delamination, was induced by embedding Teflon films during manufacturing, that were removed after. Figure 21 highlights the delamination on the CFRP beams.

The comparison for the first three natural frequencies is presented in Table 8, almost all percentage differences remained below 10%. The natural frequency is a sensitive characteristic, it is highly susceptible to slight changes in dimensions and to noise during measurement. The error could be reduced if model updating techniques were employed, however, this was not done because this level of error is acceptable for the purpose of this study.

In addition to the natural frequencies, the modes shapes were also compared.

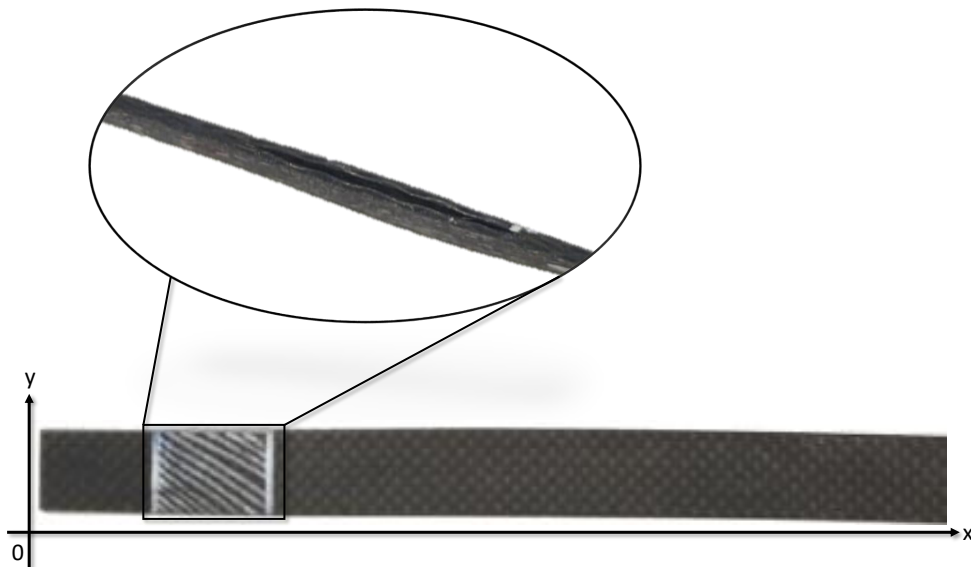


Figure 21 – Experimental specimen of the CFRP beam with the delamination highlighted.

Table 8 – Natural frequencies (in Hz) of numerical models and experimental specimens.

Specimen	Numerical			Experimental			$\Delta$   (%)		
	$\omega_1$	$\omega_2$	$\omega_3$	$\omega_1$	$\omega_2$	$\omega_3$	$\omega_1$	$\omega_2$	$\omega_3$
No damage	14.53	91.04	254.79	14.50	91.50	255.00	0.32%	0.51%	0.08%
1	15.23	92.85	255.56	16.25	101.50	278.50	6.70%	9.32%	8.98%
2	14.32	90.89	255.32	15.00	97.75	280.00	4.75%	7.55%	9.67%
3	14.39	90.88	252.49	15.00	95.50	275.00	4.24%	5.08%	8.92%
4	14.45	90.34	252.23	15.75	104.00	262.25	9.00%	15.12%	3.97%
5	14.49	89.95	254.59	15.25	99.00	263.25	5.24%	10.06%	3.40%
6	14.62	90.06	254.86	16.00	98.75	284.50	9.44%	9.65%	11.63%
7	15.02	90.52	251.51	16.50	93.00	266.50	9.85%	2.74%	5.96%
8	15.53	90.91	253.24	17.75	103.75	264.75	14.29%	14.12%	4.55%

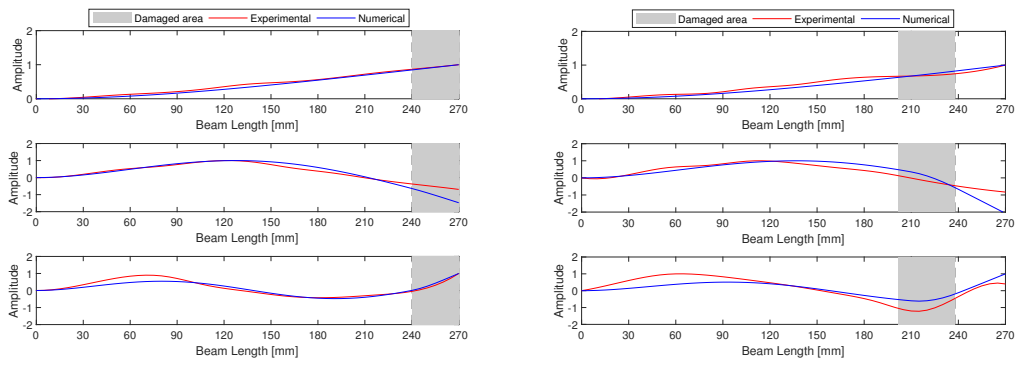
In Figure 22, both numerical and experimental mode shapes were plotted for a visual comparison. However, this plot provides only a qualitative notion of the accuracy of the model. One way to quantitatively verify is using the Modal Assurance Criterion (MAC), which is a statistic indicator that measures the degree of consistency between mode shapes [52]. The MAC is calculated through Equation 4.2, where  $\varphi_i$  and  $\varphi_j$  are the mode shapes being compared.

$$MAC = \frac{|\{\varphi_i\}^T \{\varphi_j\}|^2}{|\{\varphi_i\}^T \{\varphi_i\}| |\{\varphi_j\}^T \{\varphi_j\}|} \quad (4.2)$$

If the experimental and numerical modal shapes have high correlation, the MAC value is close to 1, whereas if they do not correlate, the MAC value is close to zero. Figure 23 presents the MAC results and indicate high correlation for same order mode shapes in numerical and experimental cases, proving that the model used is in accordance with the manufactured specimens.

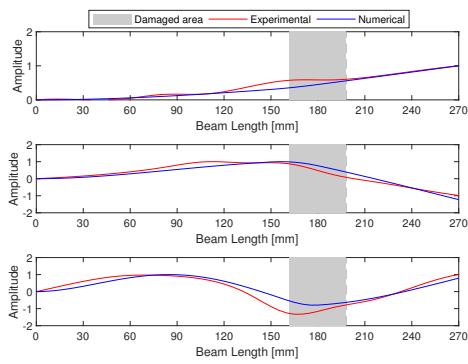
### 4.3.2 Analysis of Variance

The damage index for all components of the CCD design are shown in Figure 24, with the indexes, the responses were calculated and are presented in Table 9. The analysis of variance (ANOVA) was performed to evaluate how the damage position and severity affects the behavior on damage identification, the results are presented in Table 10. The p-value for the parameters was equal to zero in all responses, which shows that the parameters indeed explains the variance in the response. Both damage position and severity have p-value equal to zero in the the quadratic part, thus the quadratic factor is significant and the response surface will have a curvature. In the two-way interaction, the high p-value indicates that the relationship between one factor and the response does not depend on the other factor. The main effects of the factors on the average of the responses is shown in Figure 25.

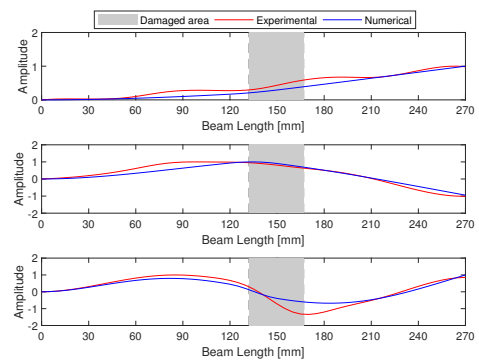


(a) Specimen 1

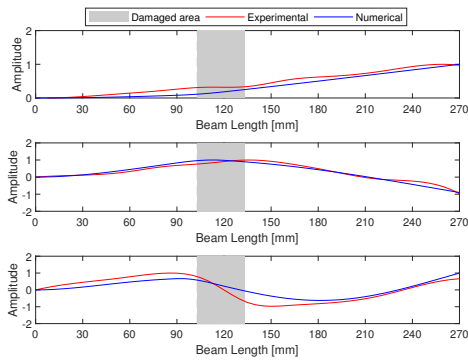
(b) Specimen 2



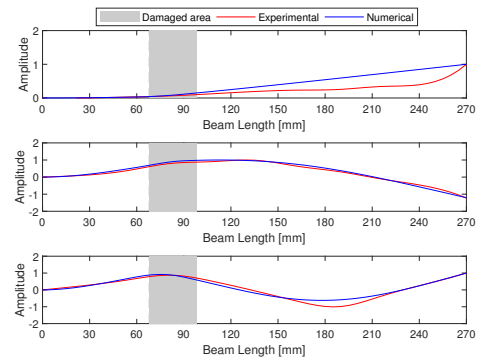
(c) Specimen 3



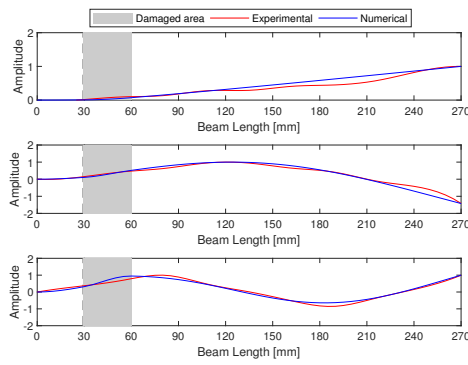
(d) Specimen 4



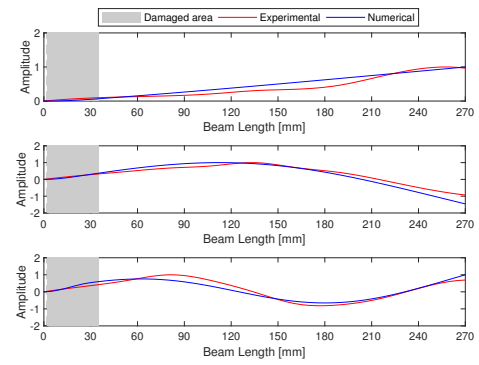
(e) Specimen 5



(f) Specimen 6



(g) Specimen 7



(h) Specimen 8

Figure 22 – Comparison between the mode shapes of the numerical models and the CFRP specimens.

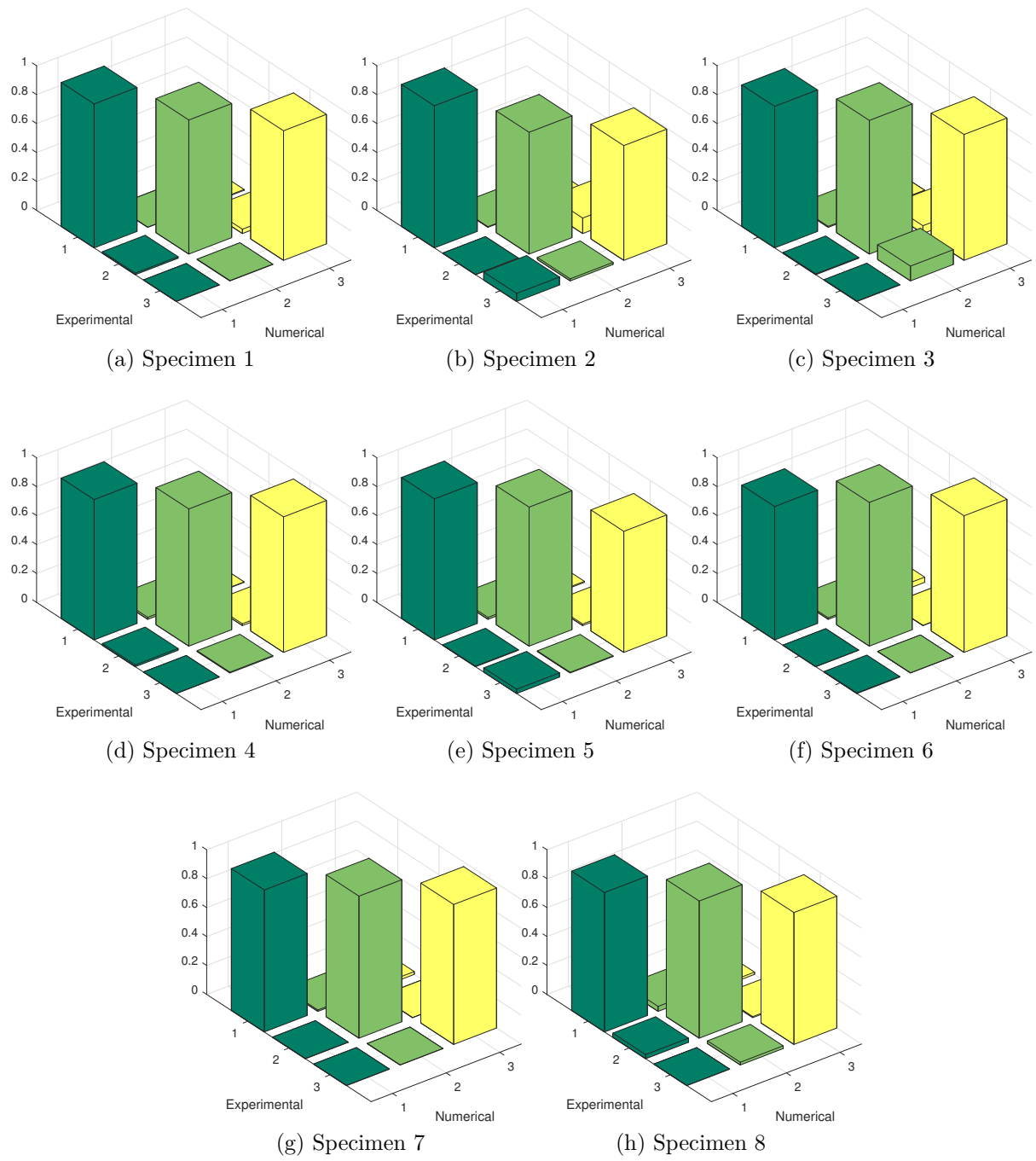


Figure 23 – Modal Assurance Criterion for comparing numerical and experimental mode shapes. Values close to one indicate high correlation.



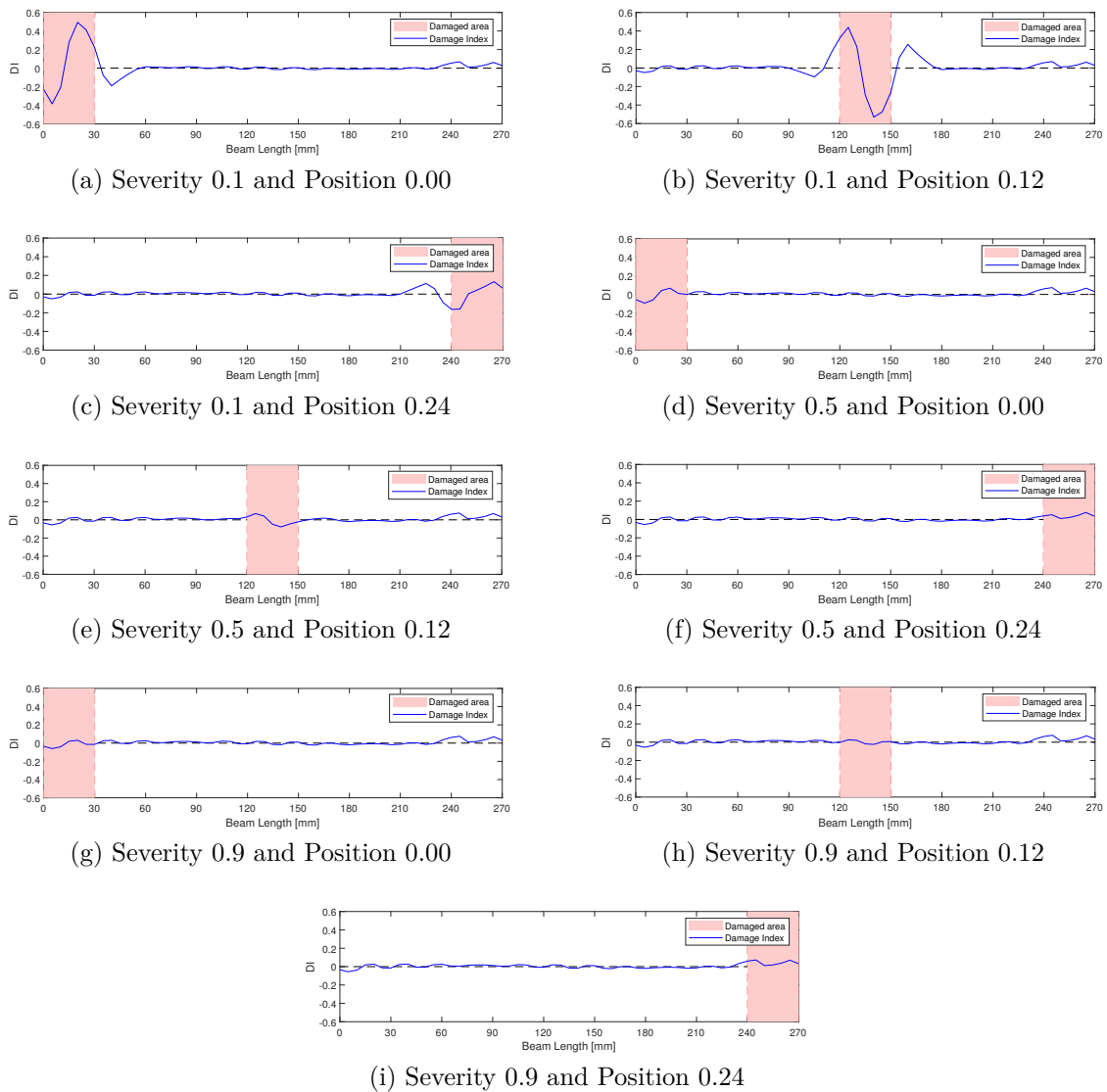


Figure 24 – Damage indexes for the components of the CCD design.

Table 9 – Response surface model considering two factors and three responses.

Variables		Responses		
Position	Severity	Peak Value	Area with Damage	Area without Damage
0.00	0.1	0.281583	10.3537	12.2699
0.24	0.1	0.424831	16.8206	5.2666
0.00	0.9	0.020756	0.9760	11.4822
0.24	0.9	0.184448	8.6856	3.8269
0.00	0.5	0.042090	1.5450	11.0486
0.24	0.5	0.206868	9.2132	3.6646
0.12	0.1	0.292807	11.4784	16.5834
0.12	0.9	0.018906	0.4909	11.9303
0.12	0.5	0.048145	1.5799	11.8134

Table 10 – Main results for the analysis of variance.

Source	p-value		
	Area with damage	Area without damage	DI Peak
<b>Model</b>	0.000	0.000	0.000
<b>Linear</b>	0.000	0.000	0.000
Position	0.000	0.000	0.000
Severity	0.000	0.018	0.000
<b>Square</b>	0.000	0.000	0.000
Position $\times$ Position	0.000	0.000	0.000
Severity $\times$ Severity	0.000	0.019	0.000
<b>2-Way Interaction</b>	0.283	0.733	0.122
Position $\times$ Severity	0.283	0.733	0.122

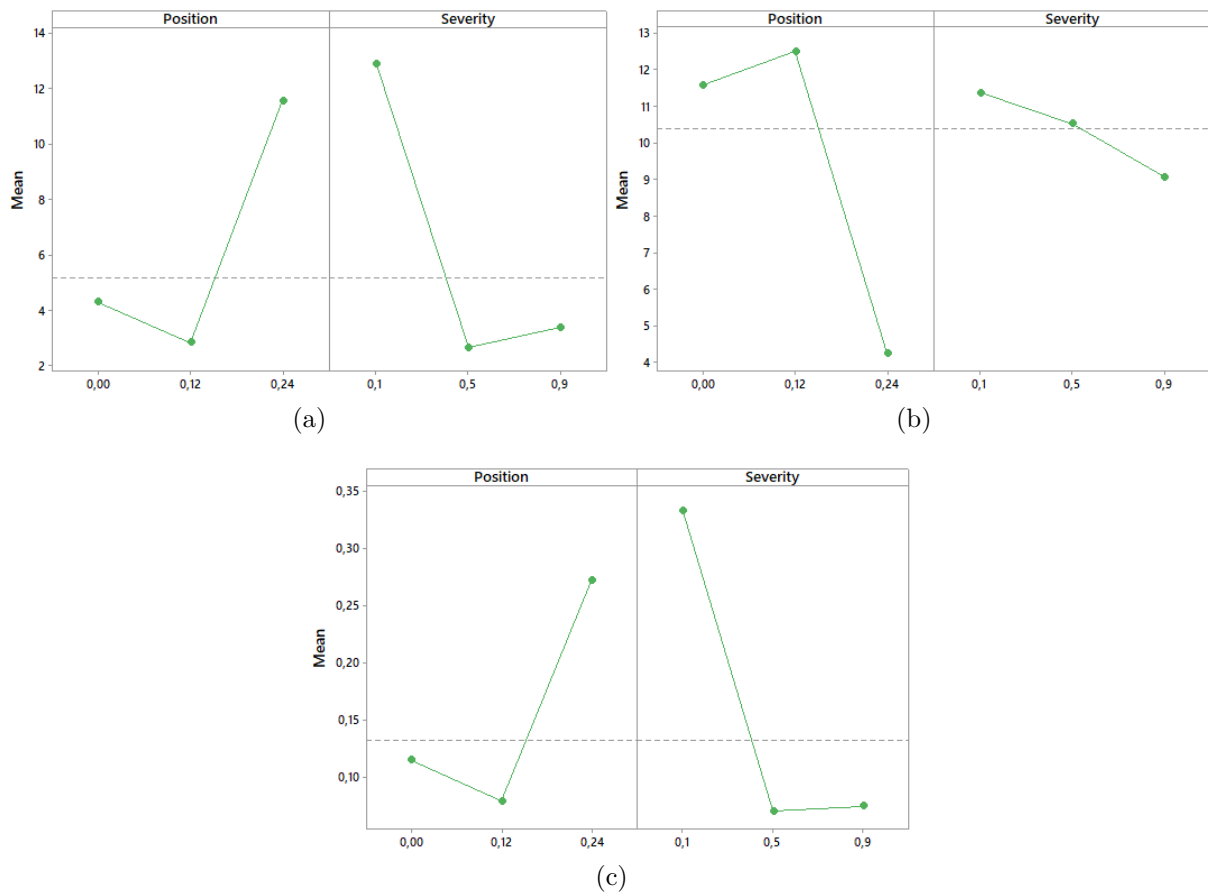


Figure 25 – Main effects plot for (a) Area with damage, (b) Area without damage and (c) damage index peak.

The Pareto's analysis is used to compare the statistical significance on main and interactions effects. This graphical technique, shown in Figure 26, presents the factors relative magnitude in decreasing order. For each response, the linear and quadratic factors have a respective importance and the two-way interaction, as expected from the high p-value, does not provide statistical significance in any response.

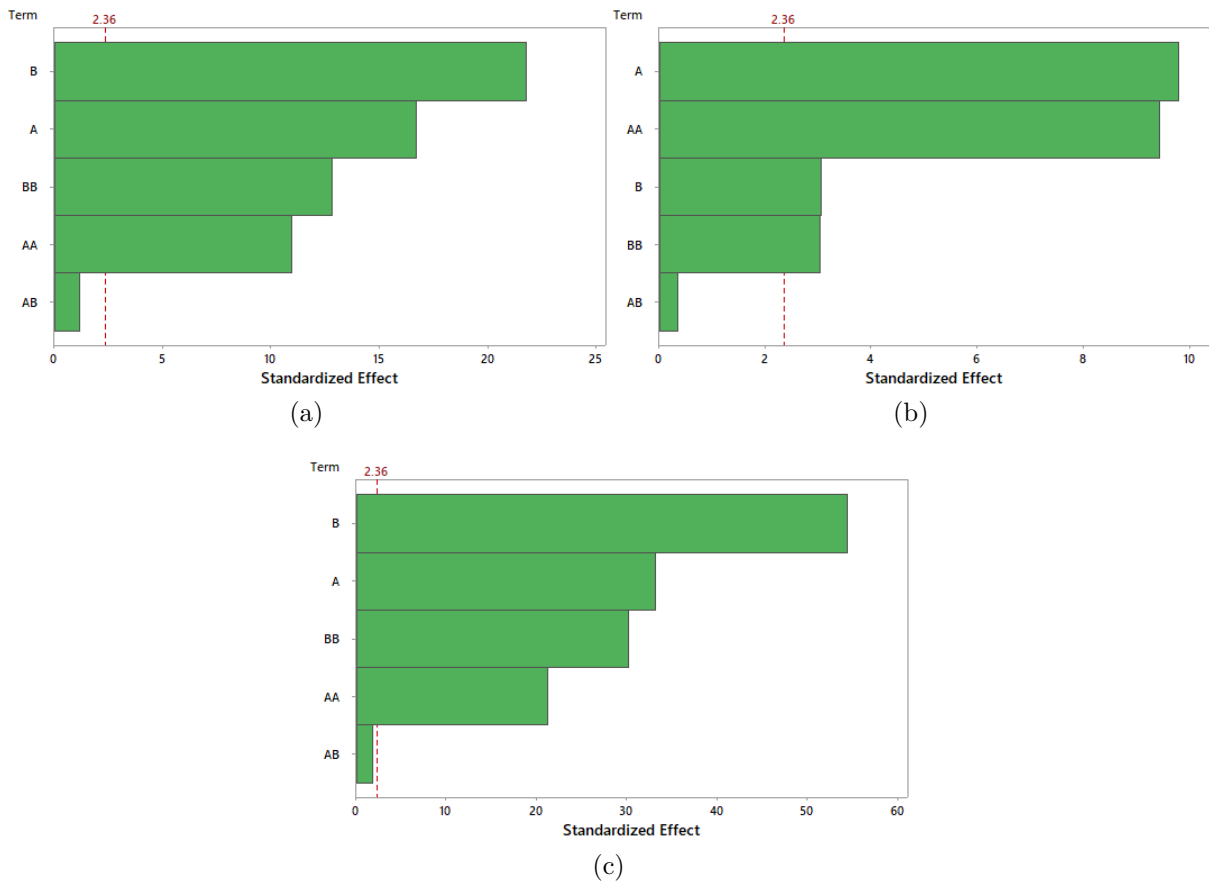


Figure 26 – Pareto's analysis for (a) Area with damage, (b) Area without damage and (c) damage index peak. Parameter A represents damage position and B represents damage severity.

### 4.3.3 Response Surface Analysis

The response surface analysis complements the ANOVA presented in the previous section. Surface plots show the entire set of possible combinations of factors and their respective response, therefore it is possible to verify the range in which the damage identification is more effective.

Some metrics are used for measuring the quality of the response surface model. Table 11 exhibits these metrics for the surfaces of the present study.  $S$  is the standard deviation of the distance between the actual data values and the adjusted values.  $R^2$  is a metric of how much the variation in a response is explained by the model and  $R^2 (adj.)$  is an adjusted version of  $R^2$  which considers the number of predictors in relation to the number of observations. The  $R^2 (adj.)$  for all responses yielded the minimum value of 94%, indicating the models are reliable.

The analysis generated the Equations 4.3 which relate the responses to the parameters position ( $x_1$ ) and severity ( $x_2$ ). These equations are the surfaces presented in

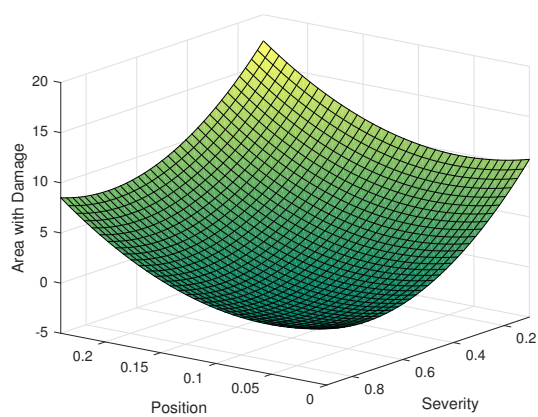
Table 11 – Model summary table for the response surface models.

Response	$S$	$R^2$	$R^2(adj.)$
Area with damage	0.534	99.43%	99.02%
Area without damage	0.919	96.53%	94.05%
Damage Index peak	0.006	99.89%	99.81%

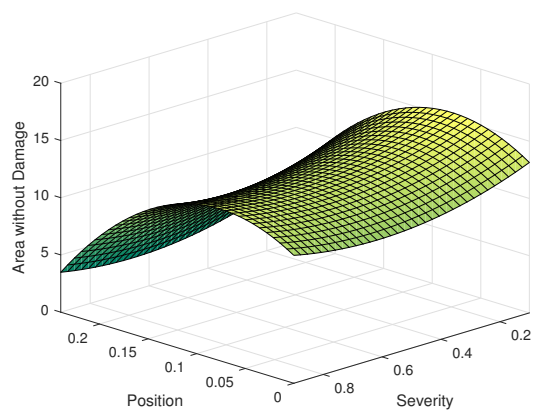
Figure 27. Since the present study analyses only the effects of two variables, they can be displayed in two axis while the response is displayed in a third axis. By analyzing Figure 27 it can be observed that both the responses for the area with damage and the DI peak have a similar behavior: a decrease in the damage severity ( $\alpha$ ) coupled with the damage positioned next to the free end of the beam provides the best results. For the area without damage, which lower values are best, the best configuration occurs for damages next to the free end of the beam and intermediate damage severity ( $\alpha$ ) values.

$$\begin{aligned}
 Y_1 &= 14.315 - 31.59 \cdot x_1 - 38.45 \cdot x_2 + 244.6 \cdot x_1^2 + 25.80x_2 \cdot x_2^2 \\
 Y_2 &= 14.33 + 58.1 \cdot x_1 - 12.94 \cdot x_2 - 362.8 \cdot x_1^2 + 10.48x_2 \cdot x_2^2 \\
 Y_3 &= 0.37732 - 0.6358 \cdot x_1 - 0.9960 \cdot x_2 + 5.157 \cdot x_1^2 + 0.6603 \cdot x_2^2
 \end{aligned} \tag{4.3}$$

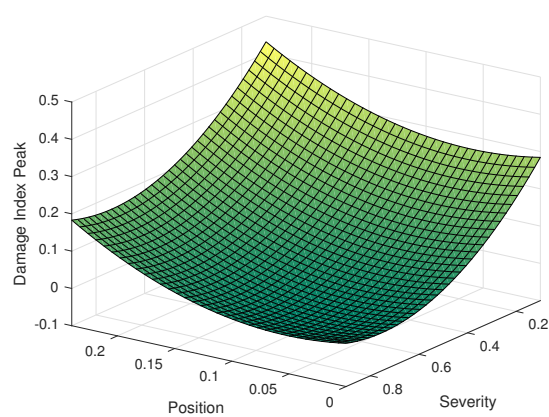
The dendrogram, presented in Figure 28, analyzes the similarity between the variables and responses. It is possible to verify a great similarity between the responses DI Peak and the Area with Damage and both responses have a similarity with the variable Damage Severity. It is also noted that the response Area without Damage has similarity with the variable Damage Position.



(a)



(b)



(c)

Figure 27 – Response surface plots for (a) Area with damage, (b) Area without damage and (c) damage index peak.

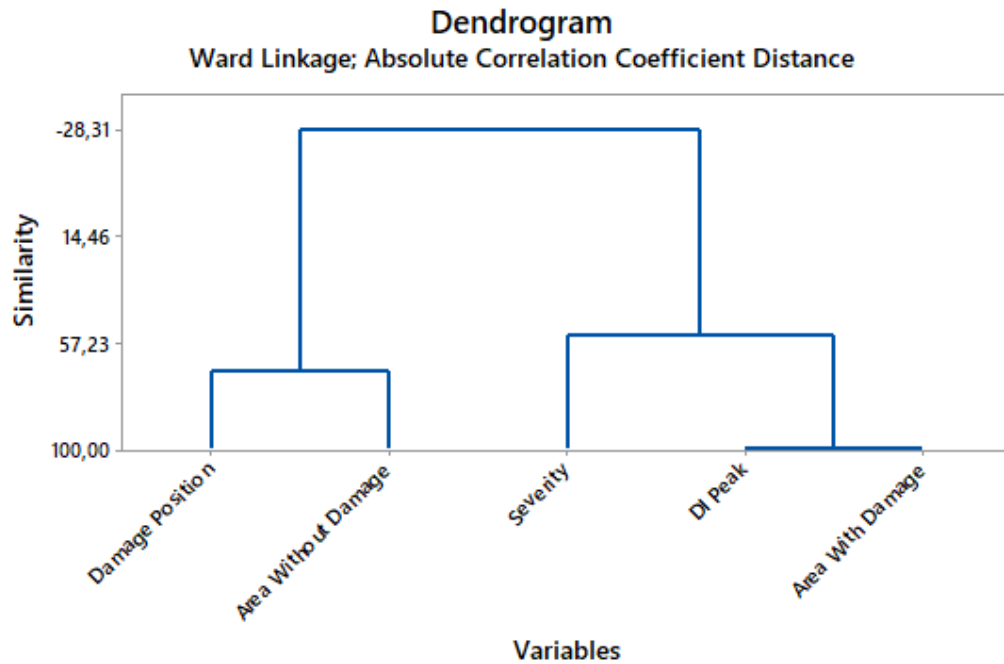


Figure 28 – Dendrogram showing the degree of similarity of the variables and responses.

## 4.4 Conclusion

In this chapter, a statistical analysis was made to assess the influence of damage characteristics in a index designed for identifying the damage. The numerical model was validated by comparison with experimental data, through techniques such as the MAC. With the response surface analysis, some insights were obtained:

- Sensitivity analysis indicated that the damage position and the level of severity influences the response differently. The best combination of these two factors for one response does not provide the desired result in other responses.
- The response for areas with damage and damage index peak, the true positives in damage identification, have similar curvatures. However, the curvature for the area without damage, the false positive in damage identification, has a different shape.
- Although the linear and quadratic factors had statistical significance in the curvature, the two-way interaction of the factors did not. Therefore, the effect of severity and damage position combined do not influence in the damage index.

## 5 General Conclusion

This study consisted in the development, optimization and testing of a damage index designed to identify damage in a composite laminated beam. In order to accomplish this objective, several steps were followed and presented in this entire dissertation.

The Discrete Wavelet Transform proved to be a robust tool for no-baseline damage identification methods. This can be stated because the damage was correctly indicated in both numerical and experimental cases. Only three mode shapes were sufficient to compose the damage index, proving that they are a reliable and easily obtainable source of information for SHM techniques.

The process for tuning the coefficients of the damage index is a well-defined methodology and was essential for the success of this study. The combination of mixture design analysis and multiobjective optimization is versatile and may be used in future works regarding damage identification. It is important to emphasize that most damage indexes proposed in the literature do not provide such clear steps for their development.

Important insights were obtained from the statistical analysis. The first is the confirmation that modelling damage through a local reduction in stiffness is a valid approach, since the dynamic characteristics of models and specimens was similar. The second is that although severity and damage position affect the response of the damage index, the effect of both factors combined does not influence the response. Finally, the response surfaces obtained illustrates how the factors influence the effectiveness of the damage index.

As suggestions for future works:

- Investigate the applicability of other wavelet function than the biorthogonal family.
- Evaluate the efficiency of the damage index in other boundary conditions of the structure.
- Further investigations are needed to test the applicability and efficiency of the presented method in more complex structures such as honeycomb composite structures or aeronautical components.
- The damage identification through strain fields can also be investigated in more depth including an numerical analysis.
- In order to enhance the performance of the proposed index, its coefficients could be considered as  $N$  unidimensional Gaussian random variables or as  $N$  components of an unique  $N$ -dimensional Gaussian random variable.

- 
- Investigate the use of different multiobjective optimization algorithms in the damage index tuning process or combine all objective functions into one and perform a single objective optimization.
  - Improve the statistical analysis by considering stochasticity and uncertainties using techniques as Principal Component Analysis, Random Fields, Polynomial Chaos Expansion, Karhunen-Loève expansion, Surrogate Models, etc.



## 6 Publications

The publications resulting out of this dissertation are listed below:

- Oliver, Guilherme Antonio; Ancelotti Junior, Antonio Carlos; Gomes, Guilherme Ferreira. Neural network-based damage identification in composite laminated plates using frequency shifts. **Neural Computing and Applications**, p. 1-12, 2020.

Impact factor: 4.774

- Oliver, Guilherme Antonio; Pereira, João Luiz Junho; Francisco, Matheus Brendon; Ancelotti Junior, Antonio Carlos; Gomes, Guilherme Ferreira. Wavelet Transform-based Damage Identification in Laminated Composite Beams. Submitted to **Engineering Structures – Journals – Elsevier** (Paper under revision)
- Oliver, Guilherme Antonio; Pereira, João Luiz Junho; Francisco, Matheus Brendon; Ancelotti Junior, Antonio Carlos; Gomes, Guilherme Ferreira. Parameter Tuning For Wavelet Transform-Based Damage Index Using Mixture Design. Submitted to **Engineering with Computers – Journals – Springer** (Paper under revision)
- Oliver, Guilherme Antonio; Pereira, João Luiz Junho; Francisco, Matheus Brendon; Ancelotti Junior, Antonio Carlos; Gomes, Guilherme Ferreira. Damage Identification In CFRP Beams Using Wavelet Transform: A Deep Statistical Analysis. Submitted to **Structures – Journals – Elsevier** (Paper under revision)

# Bibliography

- [1] Guijun Yang, Mira Park, and Soo-Jin Park. Recent progresses of fabrication and characterization of fibers-reinforced composites: A review. *Composites Communications*, 14:34–42, 2019.
- [2] Minh Quan Le, H Bainier, D Néron, C Ha-Minh, and P Ladevèze. On matrix cracking and splits modeling in laminated composites. *Composites Part A: Applied Science and Manufacturing*, 115:294–301, 2018.
- [3] Mohammad Hajikazemi, LN McCartney, and Wim Van Paepegem. Matrix cracking initiation, propagation and laminate failure in multiple plies of general symmetric composite laminates. *Composites Part A: Applied Science and Manufacturing*, 136:105963, 2020.
- [4] Guilherme Ferreira Gomes, Yohan Alí Diaz Mendéz, Patrícia da Silva Lopes Alexandrino, Sebastiao Simoes da Cunha Jr, and Antonio Carlos Ancelotti Jr. The use of intelligent computational tools for damage detection and identification with an emphasis on composites—a review. *Composite Structures*, 196:44–54, 2018.
- [5] Hossein Towsyfyhan, Ander Biguri, Richard Boardman, and Thomas Blumensath. Successes and challenges in non-destructive testing of aircraft composite structures. *Chinese Journal of Aeronautics*, 2019.
- [6] Yang Yu, Chaoyue Wang, Xiaoyu Gu, and Jianchun Li. A novel deep learning-based method for damage identification of smart building structures. *Structural Health Monitoring*, 18(1):143–163, 2019.
- [7] Rick M Delgadillo and Joan R Casas. Non-modal vibration-based methods for bridge damage identification. *Structure and Infrastructure Engineering*, 16(4):676–697, 2020.
- [8] Guilherme Ferreira Gomes, Yohan Ali Diaz Mendez, Patrícia da Silva Lopes Alexandrino, Sebastiao Simões da Cunha, and Antonio Carlos Ancelotti. A review of vibration based inverse methods for damage detection and identification in mechanical structures using optimization algorithms and ann. *Archives of Computational Methods in Engineering*, 26(4):883–897, 2019.
- [9] Sung-Wan Kim, Sung-Jin Chang, Dong-Uk Park, and Bub-Gyu Jeon. Failure criteria of a carbon steel pipe elbow for low-cycle fatigue using the damage index. *Thin-Walled Structures*, 153:106800, 2020.

- [10] Carlo Boursier Niutta, Andrea Tridello, Raffaele Ciardiello, Giovanni Belingardi, and Davide Salvatore Paolino. Assessment of residual elastic properties of a damaged composite plate with combined damage index and finite element methods. *Applied Sciences*, 9(12):2579, 2019.
- [11] Xiaohui Zhang, Jianguo Cai, and Jian Feng. Damage evaluation index of long-span spatial grid structure. In *Proceedings of IASS Annual Symposia*, volume 2019, pages 1–6. International Association for Shell and Spatial Structures (IASS), 2019.
- [12] Mohammad-Reza Ashory, Ahmad Ghasemi-Ghalebahman, and Mohammad-Javad Kokabi. Damage detection in laminated composite plates via an optimal wavelet selection criterion. *Journal of Reinforced Plastics and Composites*, 35(24):1761–1775, 2016.
- [13] Chen Yang and S Olutunde Oyadiji. Delamination detection in composite laminate plates using 2d wavelet analysis of modal frequency surface. *Computers & Structures*, 179:109–126, 2017.
- [14] Jie Zhou, Zheng Li, and Jianlin Chen. Damage identification method based on continuous wavelet transform and mode shapes for composite laminates with cutouts. *Composite Structures*, 191:12–23, 2018.
- [15] A Katunin, JV Araújo dos Santos, and H Lopes. Application of wavelet analysis to differences in modal rotations for damage identification. In *IOP Conference Series: Materials Science and Engineering*, volume 561, page 012024. IOP Publishing, 2019.
- [16] Lin-Feng Zhu, Liao-Liang Ke, Xin-Qun Zhu, Yang Xiang, and Yue-Sheng Wang. Crack identification of functionally graded beams using continuous wavelet transform. *Composite Structures*, 210:473–485, 2019.
- [17] JV Araujo dos Santos, A Katunin, and H Lopes. Vibration-based damage identification using wavelet transform and a numerical model of shearography. *International Journal of Structural Stability and Dynamics*, 19(04):1950038, 2019.
- [18] Wei Xu, Keqin Ding, Jingqiang Liu, Maosen Cao, Maciej Radzieński, and Wiesław Ostachowicz. Non-uniform crack identification in plate-like structures using wavelet 2d modal curvature under noisy conditions. *Mechanical Systems and Signal Processing*, 126:469–489, 2019.
- [19] Muyideen Abdulkareem, Abideen Ganiyu, and Muhd Z Abd Majid. Damage identification in plate using wavelet transform and artificial neural network. In *IOP Conference Series: Materials Science and Engineering*, volume 513, page 012015. IOP Publishing, 2019.

- [20] Ganggang Sha, Maciej Radzienski, Rohan Soman, Maosen Cao, Wieslaw Ostachowicz, and Wei Xu. Multiple damage detection in laminated composite beams by data fusion of teager energy operator-wavelet transform mode shapes. *Composite Structures*, 235:111798, 2020.
- [21] Rims Janeliukstis, Sandris Rucevskis, Pavel Akishin, and Andris Chate. Wavelet transform based damage detection in a plate structure. *Procedia engineering*, 161:127–132, 2016.
- [22] Muyideen Abdulkareem, Norhisham Bakhary, Mohammadreza Vafaei, Norhazilan Md Noor, and Roslli Noor Mohamed. Application of two-dimensional wavelet transform to detect damage in steel plate structures. *Measurement*, 146:912–923, 2019.
- [23] João Luiz Junho Pereira, Matheus Chuman, Sebastião Simões Cunha Jr, and Guilherme Ferreira Gomes. Lichtenberg optimization algorithm applied to crack tip identification in thin plate-like structures. *Engineering Computations*, 2020.
- [24] Guilherme Ferreira Gomes, Sebastiao Simões da Cunha, and Antonio Carlos Ancelotti. A sunflower optimization (sfo) algorithm applied to damage identification on laminated composite plates. *Engineering with Computers*, 35(2):619–626, 2019.
- [25] Guilherme Ferreira Gomes, Fabricio Alves de Almeida, Diego Morais Junqueira, Sebastiao Simões da Cunha Jr, and Antonio Carlos Ancelotti Jr. Optimized damage identification in cfrp plates by reduced mode shapes and ga-ann methods. *Engineering Structures*, 181:111–123, 2019.
- [26] Parsa Ghannadi, Seyed Sina Kourehli, Mohammad Noori, and Wael A Altabey. Efficiency of grey wolf optimization algorithm for damage detection of skeletal structures via expanded mode shapes. *Advances in Structural Engineering*, page 1369433220921000, 2020.
- [27] R Timothy Marler and Jasbir S Arora. The weighted sum method for multi-objective optimization: new insights. *Structural and multidisciplinary optimization*, 41(6):853–862, 2010.
- [28] Patricia da Silva Lopes Alexandrino, Guilherme Ferreira Gomes, and Sebastião Simões Cunha Jr. A robust optimization for damage detection using multiobjective genetic algorithm, neural network and fuzzy decision making. *Inverse Problems in Science and Engineering*, 28(1):21–46, 2020.
- [29] Guilherme Ferreira Gomes, Fabricio Alves de Almeida, Antonio Carlos Ancelotti Jr, and Sebastião Simões da Cunha Jr. Inverse structural damage identification problem in cfrp laminated plates using sfo algorithm based on strain fields. *ENGINEERING WITH COMPUTERS*, 2020.

- [30] Kaiyang Zhou, Dong Lei, Jintao He, Pei Zhang, Pengxiang Bai, and Feipeng Zhu. Single micro-damage identification and evaluation in concrete using digital image correlation technology and wavelet analysis. *Construction and Building Materials*, page 120951, 2020.
- [31] Binna Zhao, Dong Lei, Jianjun Fu, Liqun Yang, and Wenxiang Xu. Experimental study on micro-damage identification in reinforced concrete beam with wavelet packet and dic method. *Construction and Building Materials*, 210:338–346, 2019.
- [32] Yashodhya Kankanamge, Yufeng Hu, and Xiaoyun Shao. Application of wavelet transform in structural health monitoring. *Earthquake Engineering and Engineering Vibration*, 19:515–532, 2020.
- [33] P. Addison. *The Illustrated Wavelet Transform Handbook*. CRC Press, 2nd edition, 2017.
- [34] PK Basu, AB Jorge, S Badri, and J Lin. Higher-order modeling of continua by finite-element, boundary-element, meshless, and wavelet methods. *Computers & Mathematics with Applications*, 46(1):15–33, 2003.
- [35] Rodrigo Capobianco Guido, Fernando Pedroso, André Furlan, Rodrigo Colnago Contreras, Luiz Gustavo Caobianco, and Jogi Suda Neto. Cwt x dwt x dtwt x sdtwt: Clarifying terminologies and roles of different types of wavelet transforms. *International Journal of Wavelets, Multiresolution and Information Processing*, page 2030001, 2020.
- [36] Mohammadreza Vafaei, Sophia C Alih, Ahmad Baharuddin Abd Rahman, and Azlan bin Adnan. A wavelet-based technique for damage quantification via mode shape decomposition. *Structure and Infrastructure Engineering*, 11(7):869–883, 2015.
- [37] Robert L Mason, Richard F Gunst, and James L Hess. *Statistical design and analysis of experiments: with applications to engineering and science*, volume 474. John Wiley & Sons, 2003.
- [38] Douglas C Montgomery. *Design and analysis of experiments*. John wiley & sons, 2017.
- [39] S.S. Rao. *Engineering Optimization: Theory and Practice*. New Age International, 2000.
- [40] Guilherme Ferreira Gomes, Yohan Alí Diaz Mendéz, Sebastião Simões da Cunha, and Antônio Carlos Ancelotti. A numerical–experimental study for structural damage detection in cfrp plates using remote vibration measurements. *Journal of Civil Structural Health Monitoring*, 8(1):33–47, 2018.

- [41] Kalyanmoy Deb, Amrit Pratap, Sameer Agarwal, and TAMT Meyarivan. A fast and elitist multiobjective genetic algorithm: Nsga-ii. *IEEE transactions on evolutionary computation*, 6(2):182–197, 2002.
- [42] K Paul Yoon and Ching-Lai Hwang. *Multiple attribute decision making, methods and applications. Lecture Notes in Economics and Mathematical Systems*, volume 186. Springer-Verlag, 1981.
- [43] D.J. Ewins. *Modal testing: theory, practice, and application*. Mechanical engineering research studies: Engineering dynamics series. Research Studies Press, 2000.
- [44] Zhi-Fang Fu and Jimin He. *Modal analysis*. Elsevier, 2001.
- [45] Guilherme Antonio Oliver, Antonio Carlos Ancelotti, and Guilherme Ferreira Gomes. Neural network-based damage identification in composite laminated plates using frequency shifts. *Neural Computing and Applications*, pages 1–12, 2020.
- [46] Sandris Rucevskis, Rims Janeliukstis, Pavel Akishin, and Andris Chate. Mode shape-based damage detection in plate structure without baseline data. *Structural Control and Health Monitoring*, 23(9):1180–1193, 2016.
- [47] J Ciambella, A Pau, and F Vestroni. Modal curvature-based damage localization in weakly damaged continuous beams. *Mechanical Systems and Signal Processing*, 121:171–182, 2019.
- [48] Guilherme Ferreira Gomes and Rafael Simões Giovani. An efficient two-step damage identification method using sunflower optimization algorithm and mode shape curvature (msdbi-sfo). *Engineering with Computers*, pages 1–20, 2020.
- [49] Guilherme Ferreira Gomes, João Artur Souza Chaves, and Fabricio Alves de Almeida. An inverse damage location problem applied to as-350 rotor blades using bat optimization algorithm and multiaxial vibration data. *Mechanical Systems and Signal Processing*, 145:106932, 2020.
- [50] Bing Pan, Kemaq Qian, Huimin Xie, and Anand Asundi. Two-dimensional digital image correlation for in-plane displacement and strain measurement: a review. *Measurement science and technology*, 20(6):062001, 2009.
- [51] Jack PC Kleijnen. Response surface methodology. In *Handbook of simulation optimization*, pages 81–104. Springer, 2015.
- [52] Miroslav Pastor, Michal Binda, and Tomáš Harčarik. Modal assurance criterion. *Procedia Engineering*, 48:543–548, 2012.

# Appendix

# APPENDIX A – Objective Functions

In Section 2.3.4, an optimization was performed to obtain the tuned weights for the damage index. The objective functions are regressions for the areas that contain and do not contain damage in the damage index and were generated through a mixture design analysis. In total, the optimization contains eighteen objective functions that are listed below:

$$y_1 = -(0.0299 \cdot D_{1,1} + 0.1792 \cdot D_{1,2} + 1.3775 \cdot D_{1,3} + 0.0448 \cdot D_{2,1} + 1.9378 \cdot D_{2,2} + 12.8514 \cdot D_{2,3} - 0.2935 \cdot D_{1,1} \cdot D_{1,3} - 0.3551 \cdot D_{1,1} \cdot D_{2,2} - 0.5513 \cdot D_{1,1} \cdot D_{2,3} - 0.1605 \cdot D_{1,2} \cdot D_{1,3} - 0.508 \cdot D_{1,2} \cdot D_{2,2} - 0.7731 \cdot D_{1,2} \cdot D_{2,3} - 0.4503 \cdot D_{1,3} \cdot D_{2,1} - 1.4832 \cdot D_{1,3} \cdot D_{2,2} - 2.6526 \cdot D_{1,3} \cdot D_{2,3} - 0.6991 \cdot D_{2,1} \cdot D_{2,2} - 0.9783 \cdot D_{2,1} \cdot D_{2,3})$$

$$y_2 = -(0.0308 \cdot D_{1,1} + 0.3694 \cdot D_{1,2} + 2.233 \cdot D_{1,3} + 0.4016 \cdot D_{2,1} + 2.2483 \cdot D_{2,2} + 3.0408 \cdot D_{2,3} - 0.883 \cdot D_{1,1} \cdot D_{1,3} - 0.4789 \cdot D_{1,1} \cdot D_{2,2} - 0.5077 \cdot D_{1,1} \cdot D_{2,3} - 0.4377 \cdot D_{1,2} \cdot D_{1,3} - 0.3396 \cdot D_{1,2} \cdot D_{2,1} - 1.1082 \cdot D_{1,2} \cdot D_{2,2} - 1.0835 \cdot D_{1,2} \cdot D_{2,3} - 1.603 \cdot D_{1,3} \cdot D_{2,1} - 3.8182 \cdot D_{1,3} \cdot D_{2,2} - 4.1004 \cdot D_{1,3} \cdot D_{2,3} - 0.1717 \cdot D_{2,1} \cdot D_{2,2} - 0.239 \cdot D_{2,1} \cdot D_{2,3})$$

$$y_3 = -(0.0215 \cdot D_{1,1} + 0.4173 \cdot D_{1,2} + 0.6651 \cdot D_{1,3} + 0.0903 \cdot D_{2,1} + 3.998 \cdot D_{2,2} + 4.1752 \cdot D_{2,3} - 0.2709 \cdot D_{1,1} \cdot D_{1,3} - 0.4318 \cdot D_{1,1} \cdot D_{2,2} - 0.3225 \cdot D_{1,1} \cdot D_{2,3} - 0.1791 \cdot D_{1,2} \cdot D_{1,3} - 0.2497 \cdot D_{1,2} \cdot D_{2,1} - 0.9211 \cdot D_{1,2} \cdot D_{2,2} - 0.6543 \cdot D_{1,2} \cdot D_{2,3} - 0.5561 \cdot D_{1,3} \cdot D_{2,1} - 1.6234 \cdot D_{1,3} \cdot D_{2,2} - 0.6888 \cdot D_{1,3} \cdot D_{2,3} - 0.7407 \cdot D_{2,1} \cdot D_{2,2} - 0.8298 \cdot D_{2,1} \cdot D_{2,3} - 0.7215 \cdot D_{2,2} \cdot D_{2,3})$$

$$y_4 = -(0.0371 \cdot D_{1,1} + 0.2568 \cdot D_{1,2} + 0.8219 \cdot D_{1,3} + 0.2124 \cdot D_{2,1} + 1.5151 \cdot D_{2,2} + 8.2464 \cdot D_{2,3} - 0.42 \cdot D_{1,1} \cdot D_{1,3} - 0.188 \cdot D_{1,1} \cdot D_{2,1} - 0.398 \cdot D_{1,1} \cdot D_{2,2} - 0.714 \cdot D_{1,1} \cdot D_{2,3} - 0.568 \cdot D_{1,2} \cdot D_{1,3} - 0.332 \cdot D_{1,2} \cdot D_{2,1} - 0.438 \cdot D_{1,2} \cdot D_{2,2} - 1.519 \cdot D_{1,2} \cdot D_{2,3} - 0.682 \cdot D_{1,3} \cdot D_{2,1} - 1.374 \cdot D_{1,3} \cdot D_{2,2} - 2.65 \cdot D_{1,3} \cdot D_{2,3} - 1.67 \cdot D_{2,1} \cdot D_{2,2} - 2.448 \cdot D_{2,1} \cdot D_{2,3} - 0.209 \cdot D_{2,2} \cdot D_{2,3})$$

$$y_5 = -(0.0571 \cdot D_{1,1} + 0.2064 \cdot D_{1,2} + 1.5845 \cdot D_{1,3} + 0.1056 \cdot D_{2,1} + 1.4573 \cdot D_{2,2} + 15.0616 \cdot D_{2,3} - 0.656 \cdot D_{1,1} \cdot D_{2,2} - 2.234 \cdot D_{1,1} \cdot D_{2,3} - 0.728 \cdot D_{1,2} \cdot D_{1,3} - 0.492 \cdot D_{1,2} \cdot D_{2,2} - 2.654 \cdot D_{1,2} \cdot D_{2,3} - 2.552 \cdot D_{1,3} \cdot D_{2,2} - 3.801 \cdot D_{1,3} \cdot D_{2,3} - 1.092 \cdot D_{2,1} \cdot D_{2,2} - 2.059 \cdot D_{2,1} \cdot D_{2,3} - 10.689 \cdot D_{2,2} \cdot D_{2,3})$$

$$y_6 = -(0.068 \cdot D_{1,1} + 0.3108 \cdot D_{1,2} + 1.4867 \cdot D_{1,3} + 0.2659 \cdot D_{2,1} + 3.3538 \cdot D_{2,2} + 1.5728 \cdot D_{2,3} - 0.241 \cdot D_{1,1} \cdot D_{1,2} - 0.652 \cdot D_{1,1} \cdot D_{1,3} - 1.698 \cdot D_{1,1} \cdot D_{2,2} - 0.85 \cdot D_{1,1} \cdot D_{2,3} - 1.446 \cdot D_{1,2} \cdot D_{1,3} - 0.328 \cdot D_{1,2} \cdot D_{2,1} - 2.023 \cdot D_{1,2} \cdot D_{2,2} - 1.344 \cdot D_{1,2} \cdot D_{2,3} - 0.881 \cdot D_{1,3} \cdot D_{2,1} - 4.073 \cdot D_{1,3} \cdot D_{2,2} - 2.25 \cdot D_{1,3} \cdot D_{2,3} - 3.419 \cdot D_{2,1} \cdot D_{2,2} - 0.508 \cdot D_{2,1} \cdot D_{2,3} - 6.958 \cdot D_{2,2} \cdot D_{2,3})$$



$$y_7 = -(0.0546 \cdot D_{1,1} + 0.2716 \cdot D_{1,2} + 0.8035 \cdot D_{1,3} + 0.0622 \cdot D_{2,1} + 1.7467 \cdot D_{2,2} + 5.8198 \cdot D_{2,3} - 0.399 \cdot D_{1,1} \cdot D_{1,3} - 0.716 \cdot D_{1,1} \cdot D_{2,2} - 1.327 \cdot D_{1,1} \cdot D_{2,3} - 1.018 \cdot D_{1,2} \cdot D_{1,3} - 0.501 \cdot D_{1,2} \cdot D_{2,2} - 1.956 \cdot D_{1,2} \cdot D_{2,3} - 0.35 \cdot D_{1,3} \cdot D_{2,1} - 2.738 \cdot D_{1,3} \cdot D_{2,2} - 1.718 \cdot D_{1,3} \cdot D_{2,3} - 0.991 \cdot D_{2,1} \cdot D_{2,2} - 1.3 \cdot D_{2,1} \cdot D_{2,3} - 7.073 \cdot D_{2,2} \cdot D_{2,3})$$

$$y_8 = -(0.1003 \cdot D_{1,1} + 0.3035 \cdot D_{1,2} + 0.8288 \cdot D_{1,3} + 0.1503 \cdot D_{2,1} + 3.418 \cdot D_{2,2} + 11.292 \cdot D_{2,3} - 1.897 \cdot D_{1,1} \cdot D_{2,2} - 3.888 \cdot D_{1,1} \cdot D_{2,3} - 1.102 \cdot D_{1,2} \cdot D_{1,3} - 2.278 \cdot D_{1,2} \cdot D_{2,2} - 4.057 \cdot D_{1,2} \cdot D_{2,3} - 2.818 \cdot D_{1,3} \cdot D_{2,2} - 5.611 \cdot D_{1,3} \cdot D_{2,3} - 2.375 \cdot D_{2,1} \cdot D_{2,2} - 3.433 \cdot D_{2,1} \cdot D_{2,3} - 22.061 \cdot D_{2,2} \cdot D_{2,3})$$

$$y_9 = -(0.675 \cdot D_{1,1} + 2.828 \cdot D_{1,2} + 9.902 \cdot D_{1,3} + 1.055 \cdot D_{2,1} + 7.272 \cdot D_{2,2} + 25.174 \cdot D_{2,3} - 3.1 \cdot D_{1,1} \cdot D_{1,2} - 3.71 \cdot D_{1,1} \cdot D_{1,3} - 3.96 \cdot D_{1,1} \cdot D_{2,2} - 13.32 \cdot D_{1,1} \cdot D_{2,3} - 16.75 \cdot D_{1,2} \cdot D_{1,3} - 11.4 \cdot D_{1,2} \cdot D_{2,2} - 8.08 \cdot D_{1,2} \cdot D_{2,3} - 8.73 \cdot D_{1,3} \cdot D_{2,1} - 4.41 \cdot D_{1,3} \cdot D_{2,2} - 41.49 \cdot D_{1,3} \cdot D_{2,3} - 9.15 \cdot D_{2,1} \cdot D_{2,2} - 6.74 \cdot D_{2,1} \cdot D_{2,3} - 45.13 \cdot D_{2,2} \cdot D_{2,3})$$

$$y_{10} = 0.56 \cdot D_{1,1} + 2.666 \cdot D_{1,2} + 5.262 \cdot D_{1,3} + 1.299 \cdot D_{2,1} + 6.992 \cdot D_{2,2} + 17.667 \cdot D_{2,3} - 3.102 \cdot D_{1,1} \cdot D_{1,2} - 2.012 \cdot D_{1,1} \cdot D_{1,3} - 1.044 \cdot D_{1,1} \cdot D_{2,1} - 3.968 \cdot D_{1,1} \cdot D_{2,2} - 8.579 \cdot D_{1,1} \cdot D_{2,3} - 11.706 \cdot D_{1,2} \cdot D_{1,3} - 1.335 \cdot D_{1,2} \cdot D_{2,1} - 11.013 \cdot D_{1,2} \cdot D_{2,2} - 5.524 \cdot D_{1,2} \cdot D_{2,3} - 5.813 \cdot D_{1,3} \cdot D_{2,1} - 4.217 \cdot D_{1,3} \cdot D_{2,2} - 22.312 \cdot D_{1,3} \cdot D_{2,3} - 9.448 \cdot D_{2,1} \cdot D_{2,2} - 5.2 \cdot D_{2,1} \cdot D_{2,3} - 33.857 \cdot D_{2,2} \cdot D_{2,3}$$

$$y_{11} = 0.674 \cdot D_{1,1} + 3.287 \cdot D_{1,2} + 5.874 \cdot D_{1,3} + 1.638 \cdot D_{2,1} + 9.444 \cdot D_{2,2} + 16.513 \cdot D_{2,3} - 3.699 \cdot D_{1,1} \cdot D_{1,2} - 2.103 \cdot D_{1,1} \cdot D_{1,3} - 1.296 \cdot D_{1,1} \cdot D_{2,1} - 4.711 \cdot D_{1,1} \cdot D_{2,2} - 8.666 \cdot D_{1,1} \cdot D_{2,3} - 12.437 \cdot D_{1,2} \cdot D_{1,3} - 1.604 \cdot D_{1,2} \cdot D_{2,1} - 13.212 \cdot D_{1,2} \cdot D_{2,2} - 5.681 \cdot D_{1,2} \cdot D_{2,3} - 6.603 \cdot D_{1,3} \cdot D_{2,1} - 6.065 \cdot D_{1,3} \cdot D_{2,2} - 22.575 \cdot D_{1,3} \cdot D_{2,3} - 11.035 \cdot D_{2,1} \cdot D_{2,2} - 3.468 \cdot D_{2,1} \cdot D_{2,3} - 35.56 \cdot D_{2,2} \cdot D_{2,3}$$

$$y_{12} = 0.739 \cdot D_{1,1} + 2.797 \cdot D_{1,2} + 5.39 \cdot D_{1,3} + 1.837 \cdot D_{2,1} + 9.63 \cdot D_{2,2} + 17.743 \cdot D_{2,3} - 3.666 \cdot D_{1,1} \cdot D_{1,2} - 1.944 \cdot D_{1,1} \cdot D_{1,3} - 1.78 \cdot D_{1,1} \cdot D_{2,1} - 4.559 \cdot D_{1,1} \cdot D_{2,2} - 9.216 \cdot D_{1,1} \cdot D_{2,3} - 11.706 \cdot D_{1,2} \cdot D_{1,3} - 1.479 \cdot D_{1,2} \cdot D_{2,1} - 12.001 \cdot D_{1,2} \cdot D_{2,2} - 5.989 \cdot D_{1,2} \cdot D_{2,3} - 7.021 \cdot D_{1,3} \cdot D_{2,1} - 5.354 \cdot D_{1,3} \cdot D_{2,2} - 22.118 \cdot D_{1,3} \cdot D_{2,3} - 12.489 \cdot D_{2,1} \cdot D_{2,2} - 4.933 \cdot D_{2,1} \cdot D_{2,3} - 34.535 \cdot D_{2,2} \cdot D_{2,3}$$

$$y_{13} = 0.791 \cdot D_{1,1} + 2.295 \cdot D_{1,2} + 6.545 \cdot D_{1,3} + 2.026 \cdot D_{2,1} + 6.804 \cdot D_{2,2} + 20.625 \cdot D_{2,3} - 3.296 \cdot D_{1,1} \cdot D_{1,2} - 2.055 \cdot D_{1,1} \cdot D_{1,3} - 2.139 \cdot D_{1,1} \cdot D_{2,1} - 3.303 \cdot D_{1,1} \cdot D_{2,2} - 9.847 \cdot D_{1,1} \cdot D_{2,3} - 10.84 \cdot D_{1,2} \cdot D_{1,3} - 1.47 \cdot D_{1,2} \cdot D_{2,1} - 8.735 \cdot D_{1,2} \cdot D_{2,2} - 5.455 \cdot D_{1,2} \cdot D_{2,3} - 8.497 \cdot D_{1,3} \cdot D_{2,1} - 4.11 \cdot D_{1,3} \cdot D_{2,2} - 25.533 \cdot D_{1,3} \cdot D_{2,3} - 11.327 \cdot D_{2,1} \cdot D_{2,2} - 4.076 \cdot D_{2,1} \cdot D_{2,3} - 30.006 \cdot D_{2,2} \cdot D_{2,3}$$

$$y_{14} = 0.943 \cdot D_{1,1} + 2.65 \cdot D_{1,2} + 6.206 \cdot D_{1,3} + 2.455 \cdot D_{2,1} + 8.717 \cdot D_{2,2} + 23.778 \cdot D_{2,3} - 3.959 \cdot D_{1,1} \cdot D_{1,2} - 1.764 \cdot D_{1,1} \cdot D_{1,3} - 2.504 \cdot D_{1,1} \cdot D_{2,1} - 4.65 \cdot D_{1,1} \cdot D_{2,2} - 11.666 \cdot D_{1,1} \cdot D_{2,3} - 11.19 \cdot D_{1,2} \cdot D_{1,3} - 1.443 \cdot D_{1,2} \cdot D_{2,1} - 11.308 \cdot D_{1,2} \cdot D_{2,2} - 7.767 \cdot D_{1,2} \cdot D_{2,3} - 8.3 \cdot D_{1,3} \cdot D_{2,1} - 5.609 \cdot D_{1,3} \cdot D_{2,2} - 26.905 \cdot D_{1,3} \cdot D_{2,3} - 14.536 \cdot D_{2,1} \cdot D_{2,2} - 4.546 \cdot D_{2,1} \cdot D_{2,3} - 42.162 \cdot D_{2,2} \cdot D_{2,3}$$

$$\begin{aligned}
y_{15} = & 0.919 \cdot D_{1,1} + 3.657 \cdot D_{1,2} + 4.306 \cdot D_{1,3} + 2.461 \cdot D_{2,1} + 11.275 \cdot D_{2,2} + 13.033 \cdot D_{2,3} - \\
& 5.239 \cdot D_{1,1} \cdot D_{1,2} - 1.145 \cdot D_{1,1} \cdot D_{1,3} - 2.724 \cdot D_{1,1} \cdot D_{2,1} - 6.029 \cdot D_{1,1} \cdot D_{2,2} - 8.704 \cdot D_{1,1} \cdot D_{2,3} - \\
& 11.692 \cdot D_{1,2} \cdot D_{1,3} - 2.124 \cdot D_{1,2} \cdot D_{2,1} - 15.5 \cdot D_{1,2} \cdot D_{2,2} - 5.65 \cdot D_{1,2} \cdot D_{2,3} - 6.866 \cdot D_{1,3} \cdot D_{2,1} - \\
& 7.225 \cdot D_{1,3} \cdot D_{2,2} - 17.217 \cdot D_{1,3} \cdot D_{2,3} - 17.885 \cdot D_{2,1} \cdot D_{2,2} - 2.114 \cdot D_{2,1} \cdot D_{2,3} - 38.207 \cdot D_{2,2} \cdot D_{2,3}
\end{aligned}$$

$$\begin{aligned}
y_{16} = & 0.915 \cdot D_{1,1} + 5.061 \cdot D_{1,2} + 5.199 \cdot D_{1,3} + 2.116 \cdot D_{2,1} + 15.209 \cdot D_{2,2} + 19.01 \cdot D_{2,3} - 6.066 \cdot \\
& D_{1,1} \cdot D_{1,2} - 1.597 \cdot D_{1,1} \cdot D_{1,3} - 1.953 \cdot D_{1,1} \cdot D_{2,1} - 8.323 \cdot D_{1,1} \cdot D_{2,2} - 11.368 \cdot D_{1,1} \cdot D_{2,3} - \\
& 15.984 \cdot D_{1,2} \cdot D_{1,3} - 2.317 \cdot D_{1,2} \cdot D_{2,1} - 22.406 \cdot D_{1,2} \cdot D_{2,2} - 8.116 \cdot D_{1,2} \cdot D_{2,3} - 6.969 \cdot D_{1,3} \cdot D_{2,1} - \\
& 8.509 \cdot D_{1,3} \cdot D_{2,2} - 22.185 \cdot D_{1,3} \cdot D_{2,3} - 19.484 \cdot D_{2,1} \cdot D_{2,2} - 4.506 \cdot D_{2,1} \cdot D_{2,3} - 57.544 \cdot D_{2,2} \cdot D_{2,3}
\end{aligned}$$

$$\begin{aligned}
y_{17} = & 0.795 \cdot D_{1,1} + 5.374 \cdot D_{1,2} + 10.137 \cdot D_{1,3} + 1.524 \cdot D_{2,1} + 15.213 \cdot D_{2,2} + 30.597 \cdot D_{2,3} - \\
& 5.36 \cdot D_{1,1} \cdot D_{1,2} - 4.06 \cdot D_{1,1} \cdot D_{1,3} - 8.71 \cdot D_{1,1} \cdot D_{2,2} - 16.3 \cdot D_{1,1} \cdot D_{2,3} - 23.22 \cdot D_{1,2} \cdot D_{1,3} - \\
& 2.4 \cdot D_{1,2} \cdot D_{2,1} - 22.19 \cdot D_{1,2} \cdot D_{2,2} - 12.61 \cdot D_{1,2} \cdot D_{2,3} - 9.28 \cdot D_{1,3} \cdot D_{2,1} - 10.93 \cdot D_{1,3} \cdot \\
& D_{2,2} - 40.79 \cdot D_{1,3} \cdot D_{2,3} - 16.43 \cdot D_{2,1} \cdot D_{2,2} - 9.08 \cdot D_{2,1} \cdot D_{2,3} - 74.29 \cdot D_{2,2} \cdot D_{2,3}
\end{aligned}$$

$$\begin{aligned}
y_{18} = & 0.0511 \cdot D_{1,1} + 0.1917 \cdot D_{1,2} + 1.559 \cdot D_{1,3} + 0.0814 \cdot D_{2,1} + 1.0488 \cdot D_{2,2} + 6.9707 \cdot \\
& D_{2,3} - 0.586 \cdot D_{1,1} \cdot D_{1,3} - 0.269 \cdot D_{1,1} \cdot D_{2,2} - 1.218 \cdot D_{1,1} \cdot D_{2,3} - 0.995 \cdot D_{1,2} \cdot D_{1,3} - 0.44 \cdot \\
& D_{1,2} \cdot D_{2,2} - 1.506 \cdot D_{1,2} \cdot D_{2,3} - 0.603 \cdot D_{1,3} \cdot D_{2,1} - 1.656 \cdot D_{1,3} \cdot D_{2,2} - 4.584 \cdot D_{1,3} \cdot D_{2,3} - \\
& 0.276 \cdot D_{2,1} \cdot D_{2,2} - 1.359 \cdot D_{2,1} \cdot D_{2,3} - 3.435 \cdot D_{2,2} \cdot D_{2,3}
\end{aligned}$$